One of Possible Constructions of Waveguide Coupler for Superstructure

A.Zavadtsev*
MEPI, Kashirskoe Shosse 31, 115409 Moscow, Russia
*present address: DESY, MHF-SL, Notkestrasse 85, 22607 Hamburg , Germany

Abstract

This paper is devoted to the development of the design of the waveguide input coupler for RF feeding of the Superstructure for TESLA project. The first results of the calculation of the configuration of the waveguide and the drift tube of the cavities coupled with this waveguide are represented in [1]. This configuration may be recalculated and changed in accordance with all requirements of TESLA project namely the number of fed cells in the Superstructure, thermal situation, multipacting, cryomodule construction and others. The part of the coupler between feeding waveguide and the cavities is considered in this paper. HP 85180A High-Frequency Structure Simulator was used for all calculations.

1. INTRODUCTION

One of the main TESLA project requirements is the low cost. For the accelerating system it means highest effective accelerating gradient, i.e. the minimization of the length of the accelerating system parts without field. This can make the whole project cheaper. One step on this way is the Superstructure proposal [2]. But the Superstructure RF feeding question is open now.

Presently we have 40 mm coaxial coupler construction for 9 cells cavity for TTF. Next step is a proposal to feed TESLA cavities through the waveguide coupler. It decreases the number of RF channels and the length of the accelerating system without the field. The first results of this coupler calculation are in [1].

We may compare the coaxial and waveguide couplers and choose the final variant of the coupler after carrying out the following main works:

- calculation of the form and sizes of the coupler;
- calculation of the field in the coupler;
- calculation of the kick for the beam;
- construction design of the coupler in the cryomodule;
- multipacting investigation;
- cooler circuits (70 and 4 K) design, heat regime and temperature distribution calculation;
- HOM coupler design;
- design of the coupler assemblage in the cryomodule;
- design of the processes of manufacture, chemistry development, heating, tuning, assembling and high power test of the accelerating system.

The coupler should be calculated for 1.3 MW power for the feeding of two 28 cells Superstructures. The coaxial line and the coaxial ceramic window may be recalculated for increased up to 80 mm line diameter [3] without any problems. Designed Q-factor Q_{ext} for 56 cells may be got by lengthening of pin-antenna in the beam pipe and by increasing of the beam pipe diameter, which may lead to the kick increasing and to additional HOM problems correspondingly. The form and sizes of the waveguide coupler for needed Q_{ext} have been calculated already [1].

The field calculation in the filling time and in the accelerating time are needed for both coupler for the multipacting investigation and for the kick estimation correspondingly.

The feeding line of the coupler should include the first ceramic window outside the cryomodule and the second one inside the cryomodule. There is the waveguide-coaxial transition with the ceramic window in existing 40 mm coaxial coupler for 9 cells cavity. It may be recalculated for 80 mm coaxial line. Any existing rectangular waveguide window may be used as first window disposed outside the cryomodule for the waveguide coupler. The rectangular waveguide with the second ceramic window inside the cryomodule should be designed. We have one variant of this part of the coupler [1], but we should try to minimize it.

2. WAVEGUIDE CROSS-SECTION

We consider that the coupler is used for two 28 cells Superstructures, and the needed RF power is P=1.3 MW. The main parameters of the waveguide are electric field in the waveguide influencing on the multipacting and the power losses determining (together the thermoconductivity of the waveguide walls and the cooler circuits construction) the temperature distribution in the whole coupler.

The maximal electric field in the waveguide and in the coaxial line are determined by following formulas

,

$$E = 2\sqrt{\frac{PZ}{ab\sqrt{1-\left(\frac{\lambda}{2a}\right)^2}}}$$

$$E = \frac{1}{r}\cdot\sqrt{\frac{PZ}{\pi\cdot\ln\frac{R}{r}}}$$

where $Z=120\pi$ Ohm, a and b are the width and the height of the waveguide, λ is the wave length, R and r are the outside and inside conductor radiuses.

The maximal electric field E and the voltage U in the waveguide in the travelling wave regime depend on the short side b of the waveguide cross-section as this is shown in Fig.1 and 2. The multipacting chart in the rectangular waveguide in travelling wave regime is available [4].

The power loss along the line axis z is characterized by the decrement

$$\alpha = \frac{1}{2P}\cdot\frac{dP}{dz}$$

The decrement α (dB/m) is determined for the waveguide and for the coaxial line by following formulas [5]:

$$\alpha = \frac{0.793}{b\sqrt{\sigma\lambda}}\cdot\frac{1+2\cdot\frac{b}{a}\cdot\left(\frac{\lambda}{2a}\right)^2}{\sqrt{1-\left(\frac{\lambda}{2a}\right)^2}}$$

$$\alpha = \frac{0.1724}{\sqrt{\sigma\lambda}} \cdot \frac{\frac{1}{R}+\frac{1}{r}}{lg\left(\frac{R}{r}\right)}$$

where σ is the surface conductivity. The geometric sizes are in m.

The α(b) dependence in relative values is represented in Fig.3. Comparing the power loss in the waveguide coupler with the power loss in the coaxial coupler [3] we should note that α=1.79 in the same relative values for the coaxial line with outside conductor diameter 80 mm and impedance 80 Ohm including loss in the inside conductor α_{in}=1.41 and in the outside conductor α_{out}=0.37. But the inside conductor is connected to 70K parts of the cryomodule and the outside conductor is connected to the cavity. Therefore we should take into account α_{out} only comparing the coaxial coupler with the waveguide one.

The heat losses in the waveguide is higher then in the outside conductor of 80 mm coaxial line. But we should calculate the admissible losses taking into account the real construction of the coupler and the cooler circuits connected to the nitrogen and helium channels. If the 30 mm waveguide coupler construction will be impossible, we may consider value b increased up to 50 mm for example.

It will lead to increasing of the coupling of the waveguide with the cavities or to decreasing of Q_{ext}. The waveguide has special bent short surface to increase Q_{ext} [1]. Additional increasing Q_{ext} may be made up at least by three ways:

A. The distance between the waveguide and the cavity may be increased (for one Superstructure).

B. The short surface may be bent more (increased angle α [1]).

C. The diameter of the drift tube connected with the waveguide may be decreased.

D. The position of the plane short in the waveguide at $\Lambda/4$ from the cavity axis corresponds to minimum of Q_{ext}, where Λ is the wave length in the waveguide. Q_{ext} increases infinitely at $\Lambda/2$ position of the short. Q_{ext} changes very quickly with the plane short moving around $\Lambda/2$. We may install the rectangular bellow between the cavities and the plane short to control the value Q_{ext} moving the plane short. $\Lambda/2$=161 mm. Therefore the bellow with the plane short will be inside 4K region in the cryomodule. But we should take into account the field increasing in this part of the waveguide.

The parameters of the waveguides and the coaxial line corresponding to P=1.3 MW are represented in Table 1. dP/dz is power loss per 1 cm in the transmission line. The power 1.3 MW corresponds to the feeding of two 28 cells Superstructures. 0.65 MW is needed for one 28 cells Superstructure. It was assumed that these line material is the stainless steel covered by the copper with the conductivity $\sigma=5.8*10^7$ $(Ohm*m)^{-1}$ at room temperature and σ is proportional to 1/T (T is temperature in K). The pulse duration is 1330 μs. The repetition rate is 5 Hz.

The waveguide or the outer conductor of the coaxial line are disposed between the cool window at 70 K and the cavity input flange at 4 K. Therefore the conductivity σ, the decrement α and the power loss per length unit change along the transmission line between values corresponding to 70 and 4 K. The inner conductor of the coaxial line is at 70 K.

Table 1: Feeding lines parameters.

Feeding line	E, kV/cm	U, kV	α, 10^{-3} dB/m at room temperature	dP/dz, W/cm at 1.3 MW; in cryomodule
Waveguide 165.1x82.55mm	4.48	37.0	5.46	0.11-0.46
Waveguide 165.1x50 mm	5.76	28.8	7.85	0.16-0.66
Waveguide 165.1x30 mm	7.44	22.3	11.9	0.24-1.00
Coaxial line 80 mm 80 Ohm inner conductor outer conductor	10.3	14.4	9.76 7.72 2.04	 0.65 0.041-0.17

3. CERAMIC WINDOW

3.1. Variant 1

The main requirements of the ceramic window are:

- the window should have minimal sizes because it will be install into the cryomodule;
- the ceramic should not be seen from the beam axis;
- the electric field in the window should be minimized.

The variant 1 of the window is shown in Fig.4 and 5.

The window consists of the cylindrical cavity with plane ceramic and input and output waveguides with 165.1x30 mm cross-section coupled with the cavity through the slots with sizes hx30 mm.

The power transmission through the window is

$$K = \frac{4\beta_1\beta_2}{(1+\beta_1+\beta_2)^2} \cdot \frac{1}{1+\left(\frac{2Q_0\Delta f}{(1+\beta_1+\beta_2)f}\right)^2}$$

where β_1 and β_2 are the coupling coefficients of the cavity with input and output waveguides, Q_0 is own Q-factor of the cavity, Δf is frequency shift.

Analysing last equation one can say that

- the power transmission is equal to 1 at resonance frequency if $\beta_1 = 1+\beta_2$;
- the window has more broad frequency band for larger β_1 and β_2.

Therefore it is better to make $\beta_1 >> 1$ and $\beta_2 >> 1$. The good matching may be got for $\beta_1 = \beta_2$ in this case. It means that the window may be symmetrical about the window centre.

The reflection S_{11} from the window for h=90 mm and matched output waveguide in the frequency region 1.0-1.6 GHz is shown in Fig.6 and 7 (Smith chart).

There are three resonances corresponding to TM_{010}- (1.155 GHz), TE_{111}- (1.225 GHz) and TE_{211}-mode (1.400 GHz) in this frequency region. The window is matched at each this res-

onance. But the frequency bandwidths are small especially at TE_{111}-mode, and the electric field in the ceramic is large (12.3 kV/cm for TM_{010}- and 11.0 kV/cm for TE_{212}-mode; the electric field corresponds to 1.3 MW power here and go on).

The variation of the cavity sizes and the size h of the coupling slots allowed to get the window variant in which the field is a superposition of these three modes TM_{010}, TE_{111} and TE_{211} at operating frequency 1.3 GHz.

$S_{11}(f)$ dependence of this variant is shown in Fig.8 and 9 (Smith chart). The phase of S_{11} as function of the frequency is shown in Fig.10.

The electric field distribution in the window in different cross-sections is shown in Fig.11, 12 and 13. The relative field distribution does not change in the usual resonator in time. The field value changes only. The field moves in designed window cavity. This may be seen in Fig.14, 15 and 16, where the field distributions in the window for input signal phase 0^0, 30^0 and 90^0. The field behaviour in the window cavity is more similar to the field behaviour in the transmission line rather then in the resonator.

One can see that the maximal electric field in the ceramic is equal to 5.0 kV/cm, i.e. less then in the waveguide.

3.2. Variant 2

The variant 2 of the window with 165.1x82.55 mm cross-section of input and output waveguides was calculated also. This window is shown in Fig.17 and 18. The coupling slots between the waveguides and the cavity have the sizes 165.1x30 mm, i.e. no diaphragms are used in the waveguides (h=165.1 mm).

$S_{11}(f)$ dependence is shown in Fig.19 and 20 (Smith chart). The S_{11} phase depending on the frequency is shown in Fig.21.

The field distribution in three planes is shown in Fig.22, 23 and 24 at the input signal phase corresponding to the maximal field in the cavity. Maximal field in the ceramic is equal to 6.7 kV/cm. Maximal electric field in the window is located on the edges between the waveguide and the cavity and equal to 22.5 kV/cm. This value is higher then in variant 1, but it is too low for high power breakdown.

4. WAVEGUIDE TRANSITIONS

4.1. 82.55-30 mm transition

The waveguide transition from 165.1x82.55 mm to 165.1x30 mm cross-section is needed to connect:

- 165.1x82.55 mm waveguide from generator with 165.1x30 mm input waveguide of the window variant 1;
- 165.1x82.55 mm output waveguide of the window variant 2 with 30 mm coupler of the accelerating system.

Two steps waveguide transport and its $S_{11}(f)$ dependence are shown in Fig.25 and 26.

4.2. 30-30 mm S-bend

The waveguide S-bend with constant waveguide cross-section 165.1x30 mm is needed to connect the output waveguide of the window variant 1 with 30 mm coupler of the accelerating system and that the ceramic of the window is not seen from the beam axis.

30-30 mm S-bend and its $S_{11}(f)$ dependence are shown in Fig.27 and 28.

4.3. 30-50 mm S-bend

This S-bend is like the 30-30 mm S-bend, but it may be used with 50 mm coupler. 30-50 mm S-bend and its $S_{11}(f)$ dependence are shown in Fig.29 and 30.

5. COMMON VIEW OF THE COUPLER

The common views of the coupler with windows variant 1 and 2 are shown in Fig.31 and 32.

6. CONCLUSION

Proposed constructions of input coupler have following properties:

- minimal sizes; the ceramic window is disposed inside the waveguide practically;
- low electric field in the ceramic;
- admissible frequency band (window and waveguide transitions);
- ceramic is not seen from beam axis

The final construction of the coupler may be chosen after carried out the works described in part 1.

7. REFERENCES

1. M.Dohlus, A.Gamp, H.Hartwig, N.Holtkamp, A.Jostingmeier, C.Martens, M.Marx, C.Pagani, J.Weisend, V.Kaljuzhny, K.Jin, A.Zavadtsev, S.Yarigin. Status of Waveguide Coupler Activity at DESY. The TTF Coupler Meeting, Saclay, October 19-20, 1998. November 1998, TESLA 98-28.

2. J.Sekutowicz. Status of Superstructure Studies. The TTF Coupler Meeting, Saclay, October 19-20, 1998. November 1998, TESLA 98-28.

3. D.Proch. Coaxial Coupler for Superstructures. The TTF Coupler Meeting, Saclay, October 19-20, 1998. November 1998, TESLA 98-28.

4. D.Proch. Multipactor Simulations. The TTF Coupler Meeting, Saclay, October 19-20, 1998. November 1998, TESLA 98-28.

5. A.L.Feldstein, L.R.Javich, V.P.Smirnov. Reference Book on Waveguide Technics Elements. GEI, Moscow-Leningrad, 1963.

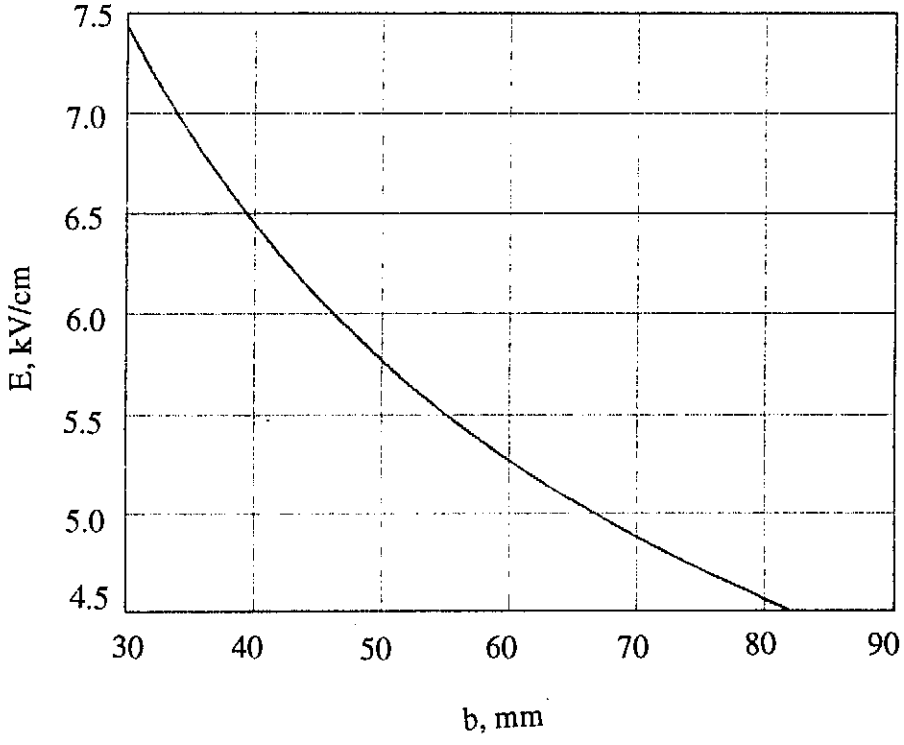

Fig.1. Maximal electric field E in the waveguide with the cross-section 162xb at power P=1.3 MW.

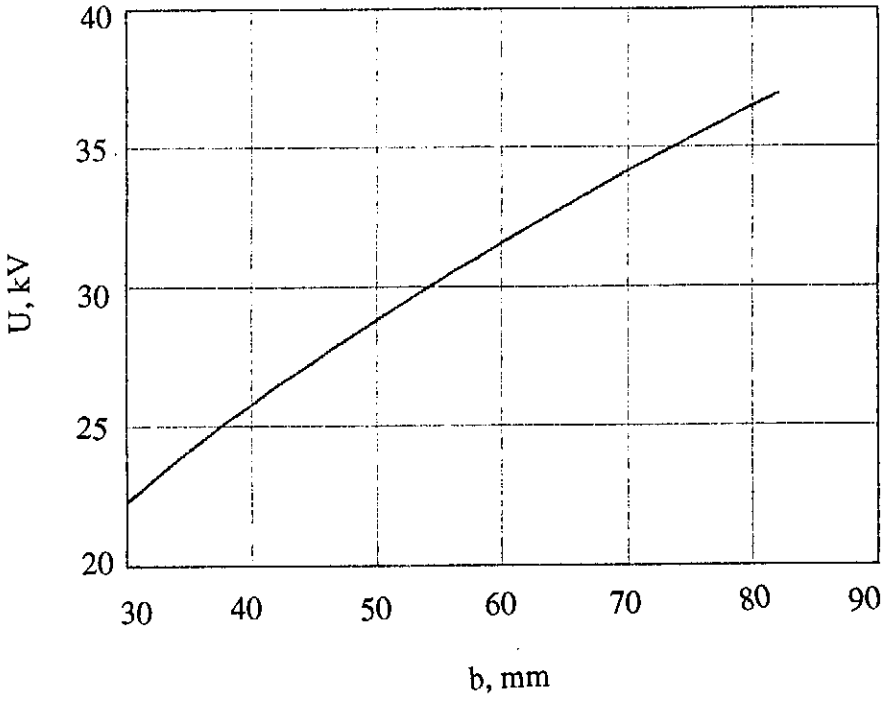

Fig.2. The voltage U in the waveguide with the cross-section 165xb at power P=1.3 MW.

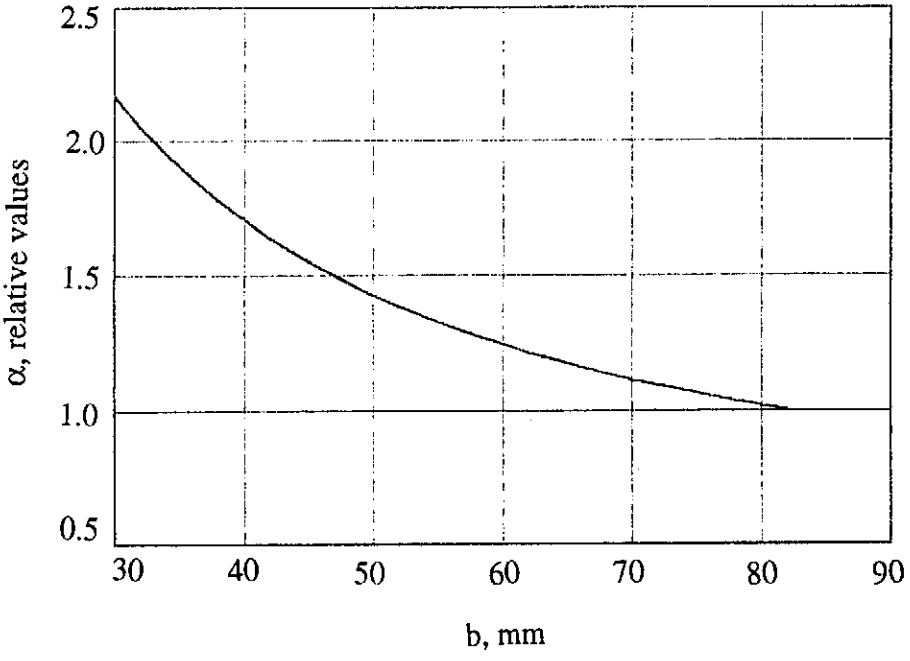

Fig.3. The decrement α depending on b.

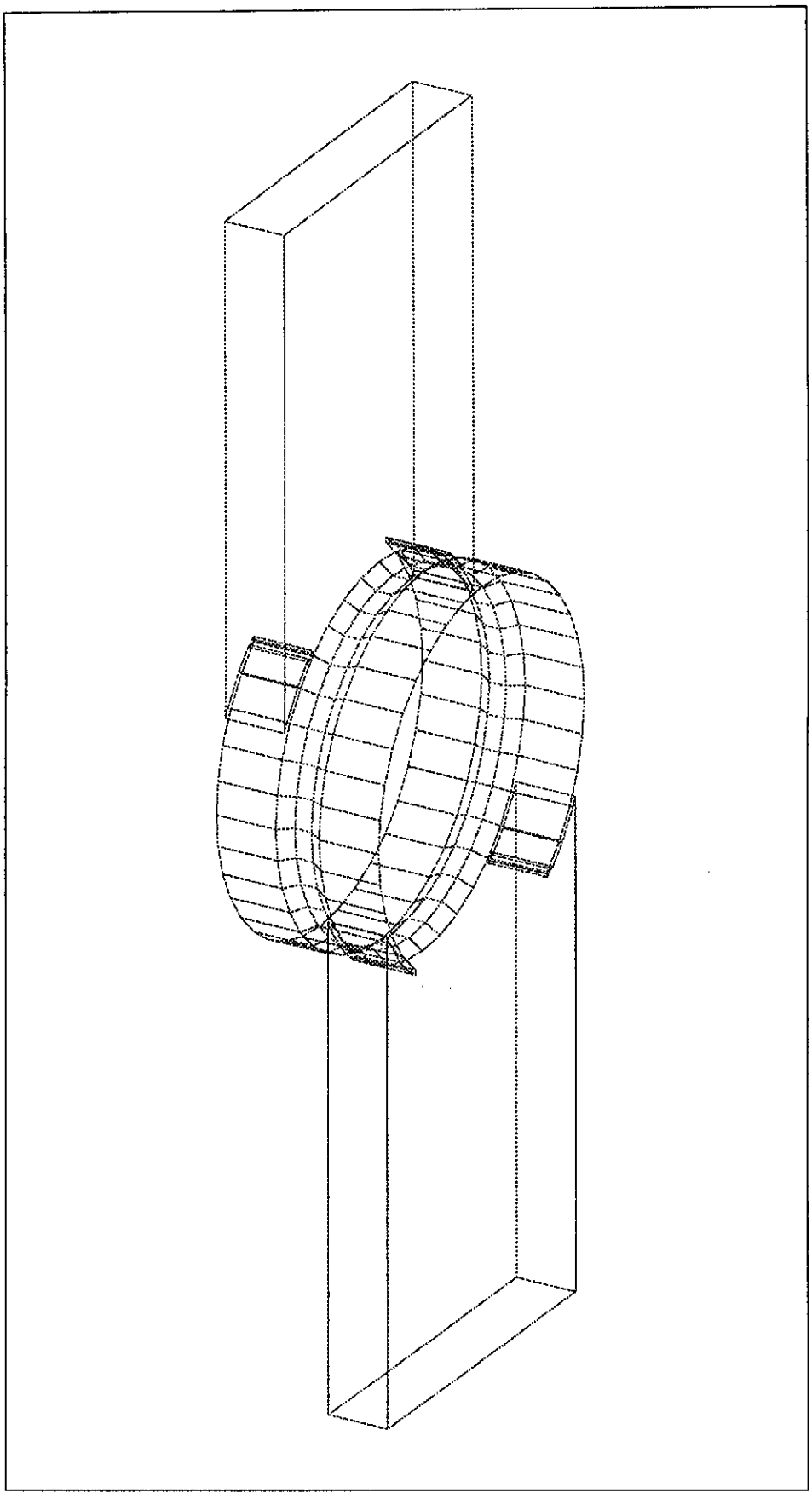

Fig.4. Variant 1 of the window.

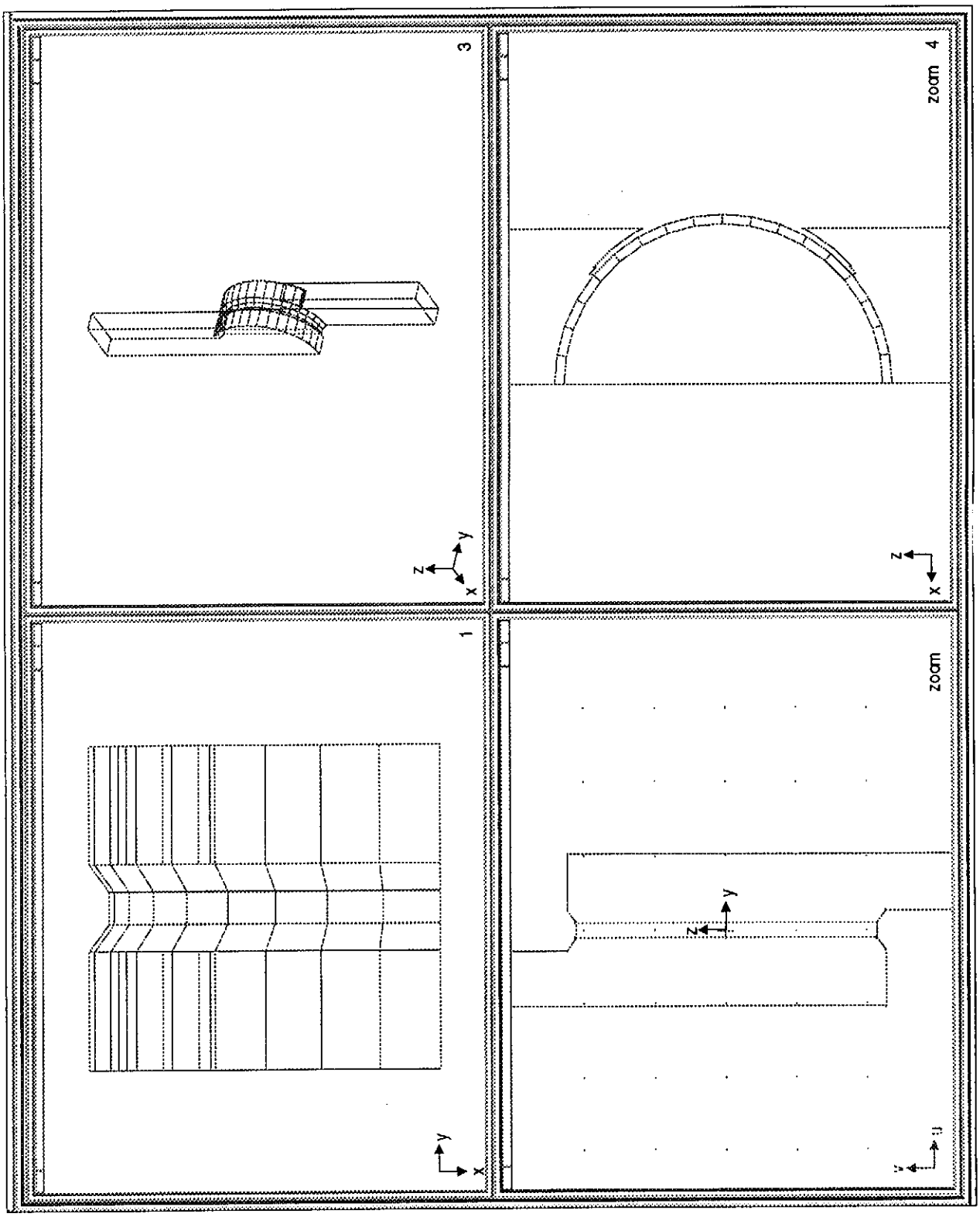

Fig.5. Variant 1 of the window.

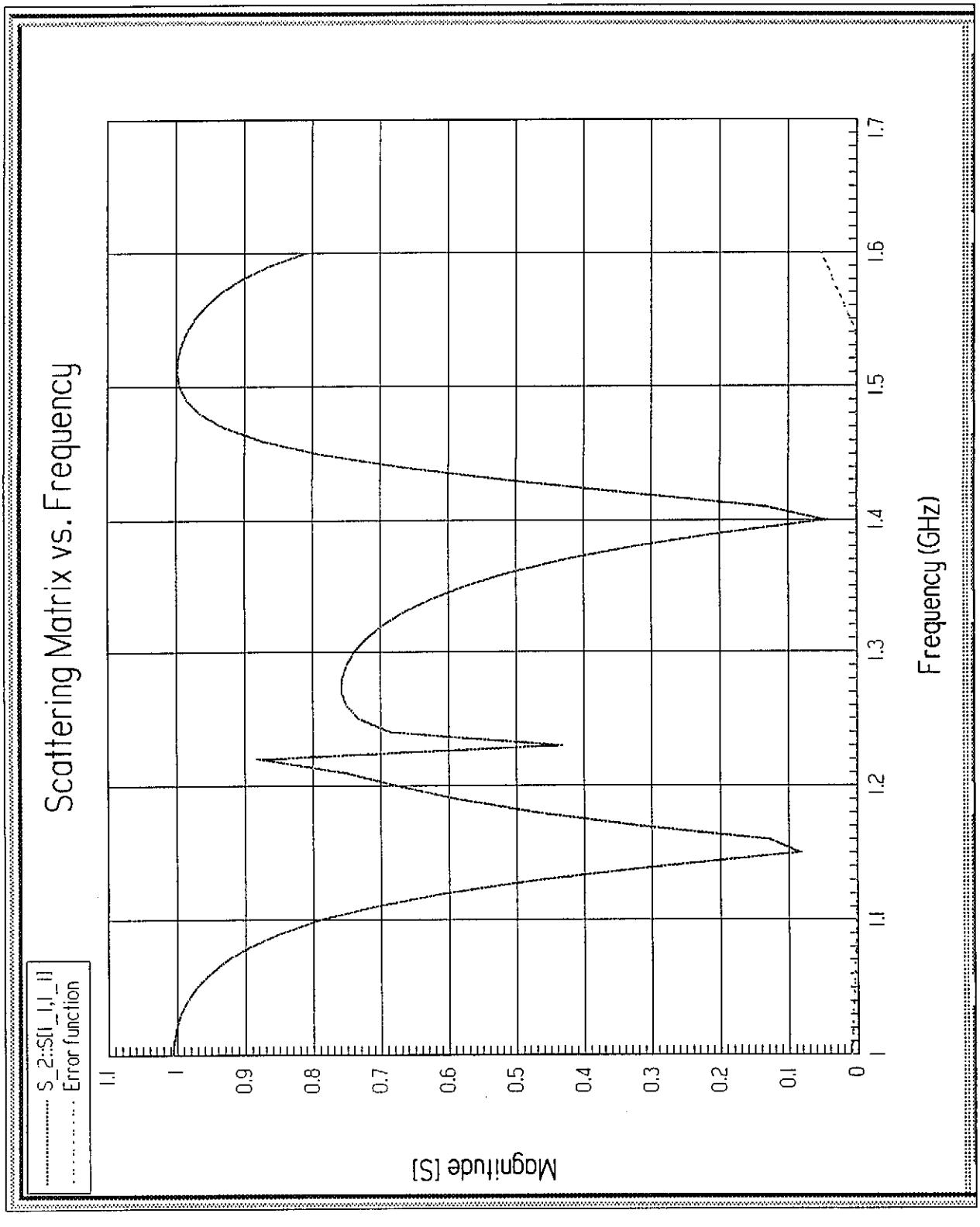

Fig.6. $S_{11}(f)$ dependence for window variant 1 with h=90 mm.

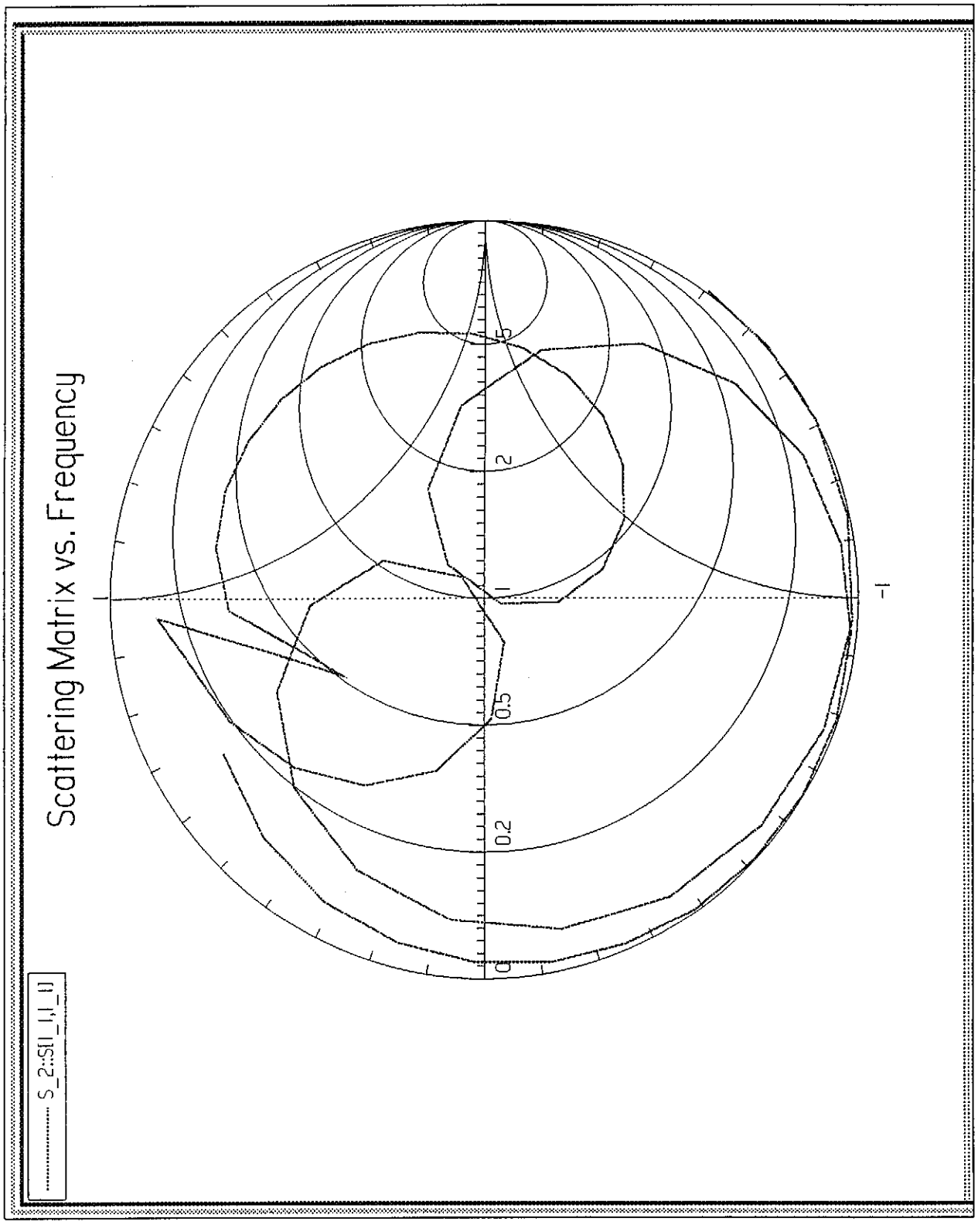

Fig.7. $S_{11}(f)$ dependence in Smith chart for window variant 1 with h=90 mm.

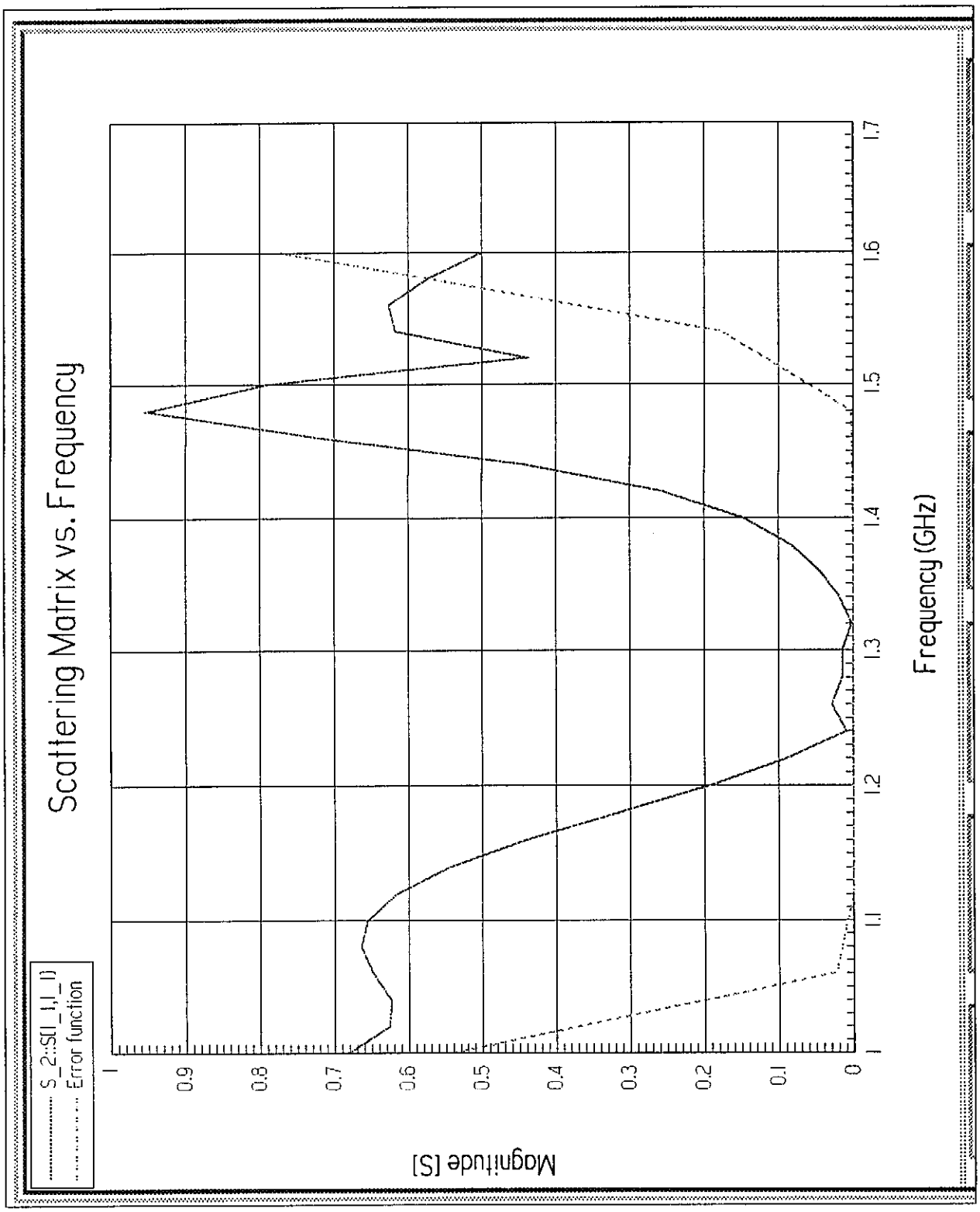

Fig.8. $S_{11}(f)$ dependence for window variant 1 with h=114 mm.

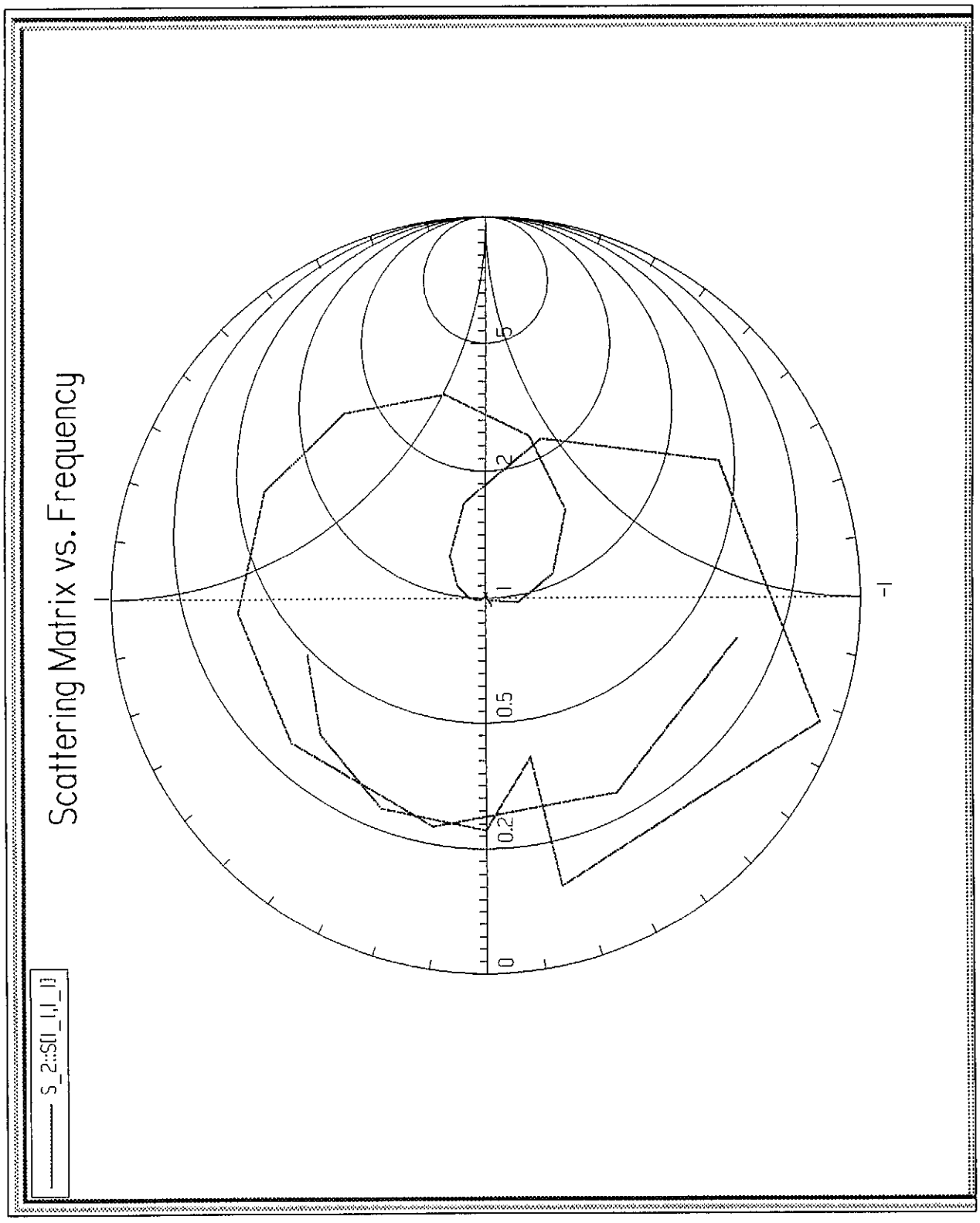

Fig.9. $S_{11}(f)$ dependence in Smith chart for window variant 1 with h=114 mm.

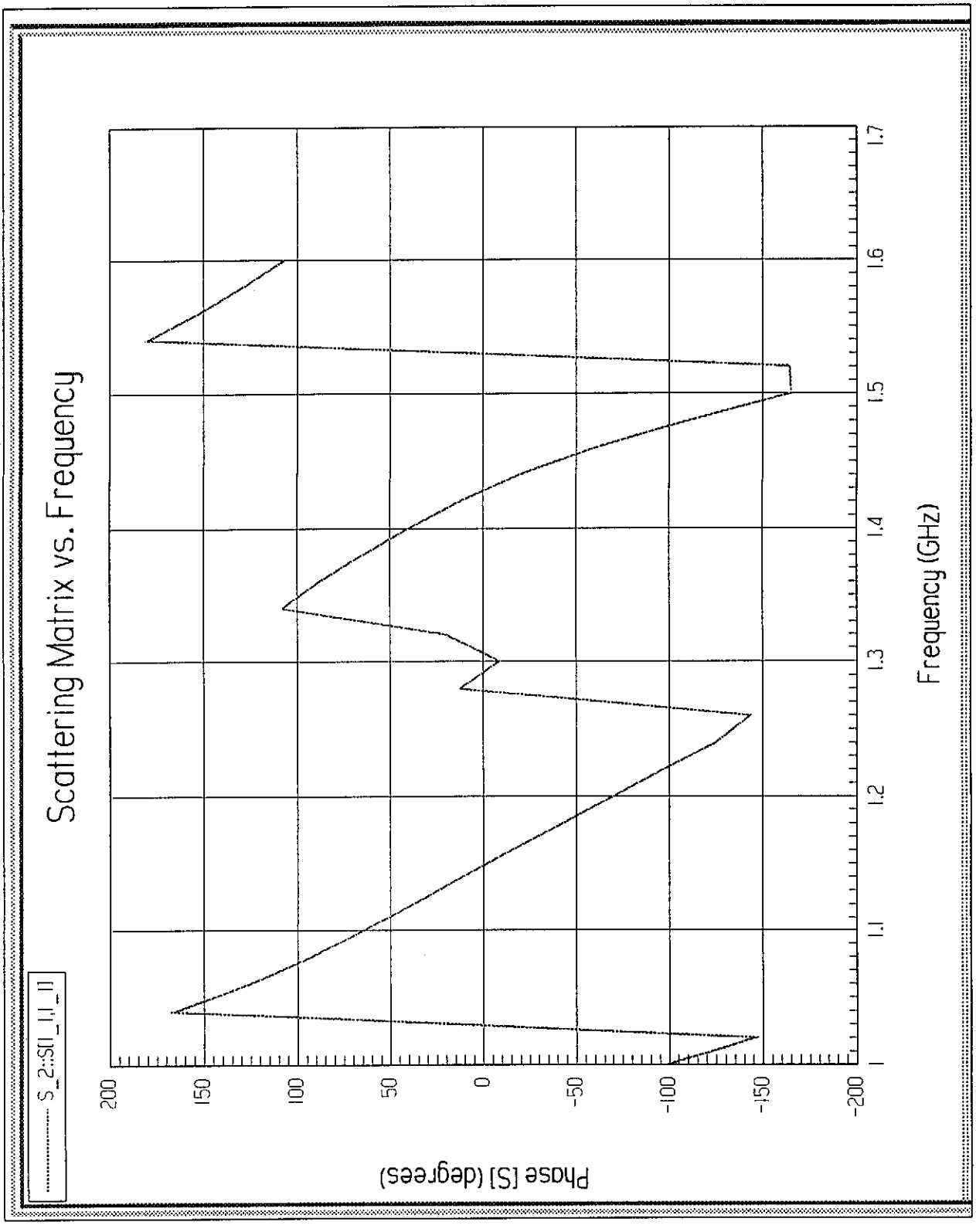

Fig.10. S_{11} phase dependence on frequency for window variant 1 with h=114 mm.

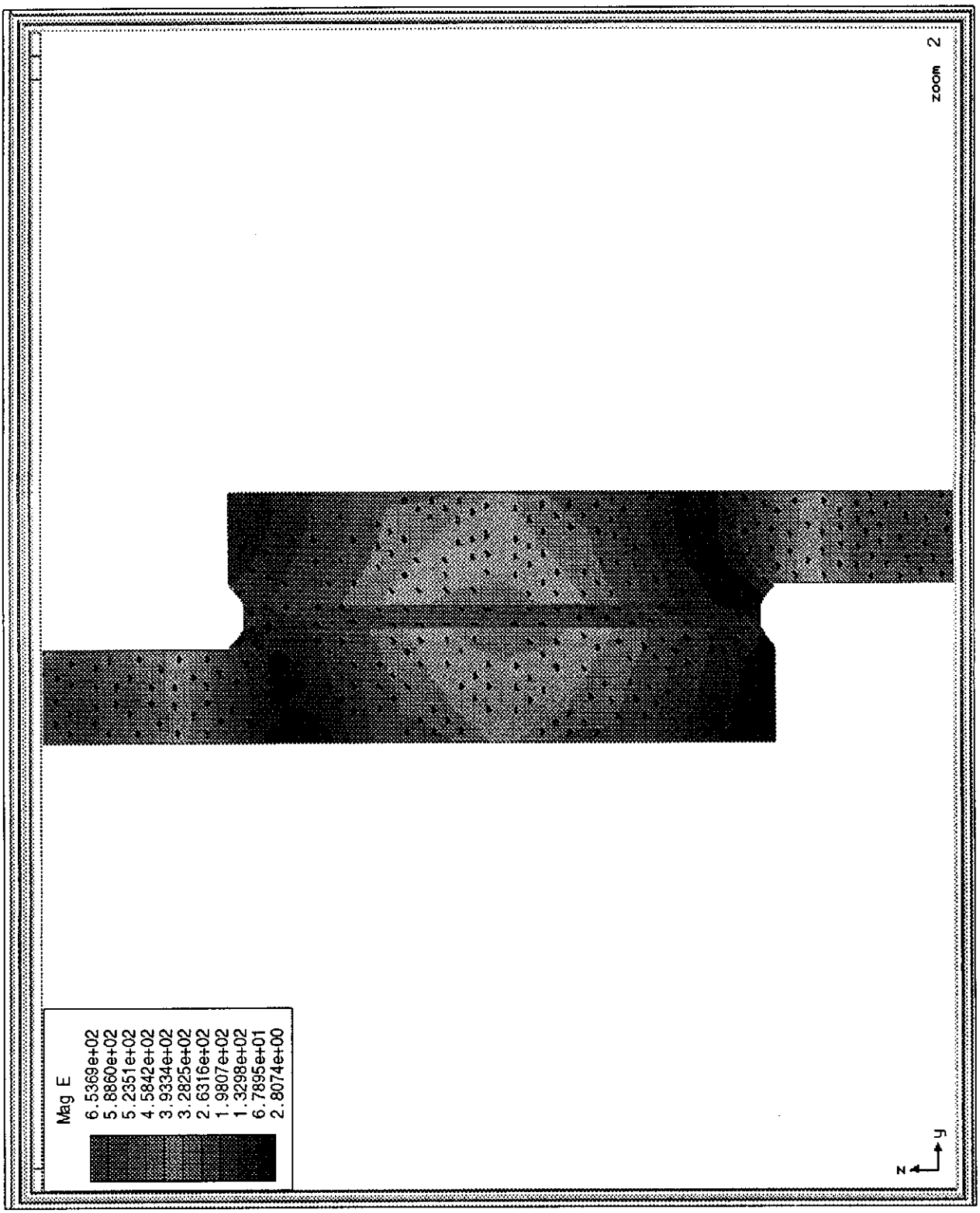

Fig.11. Electric field distribution in the window variant 1.

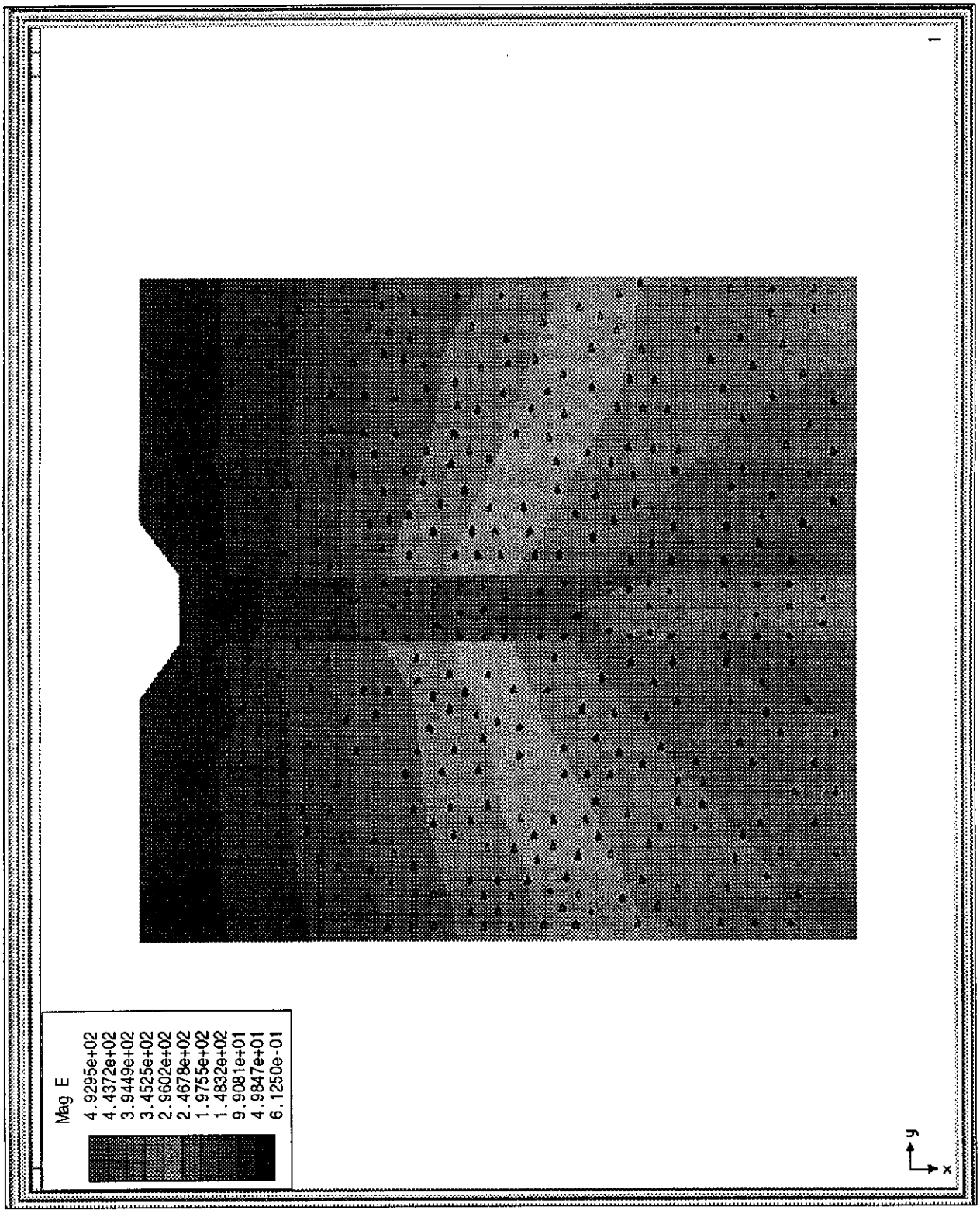

Fig.12. Electric field distribution in the window variant 1.

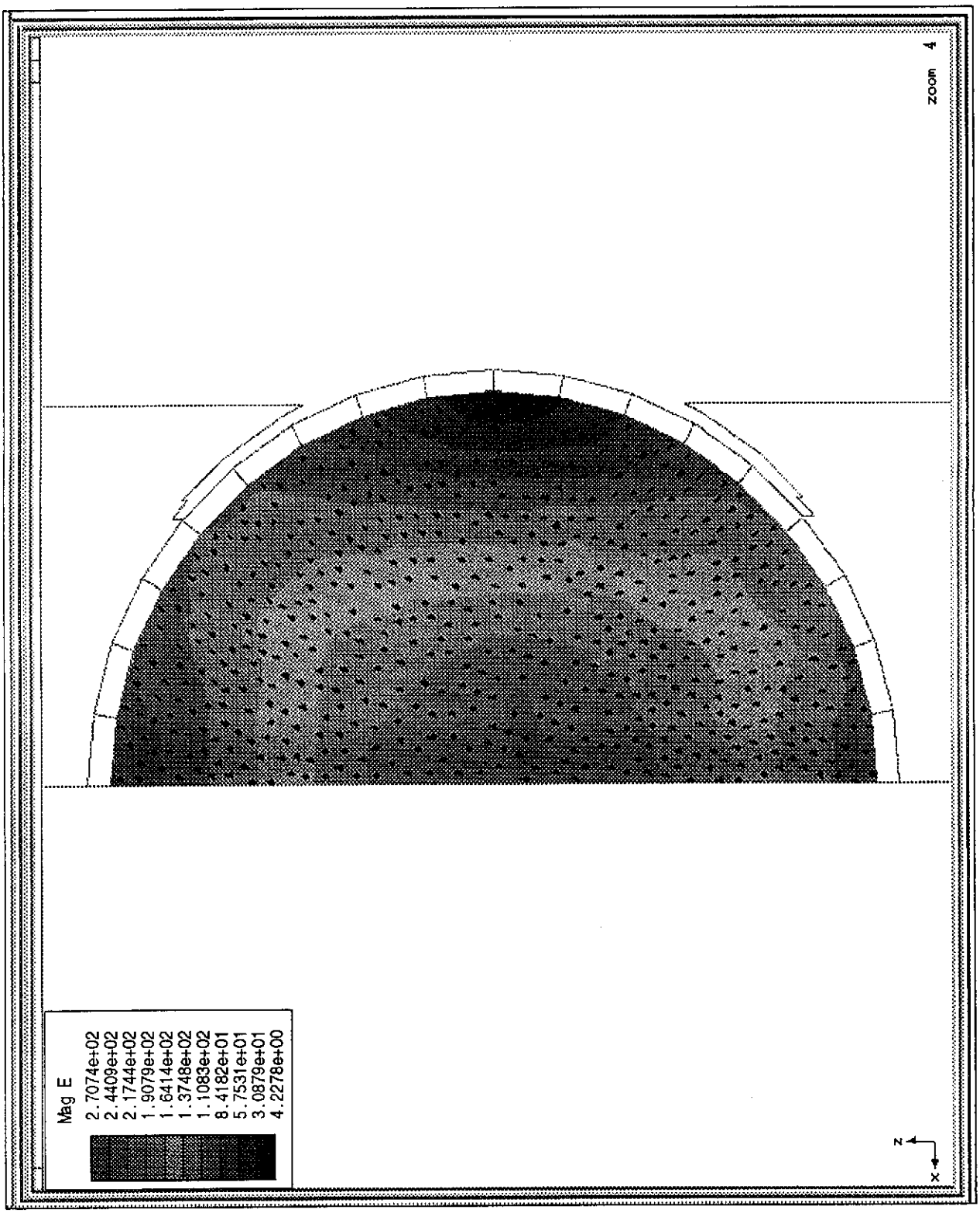

Fig.13. Electric field distribution in the window variant 1.

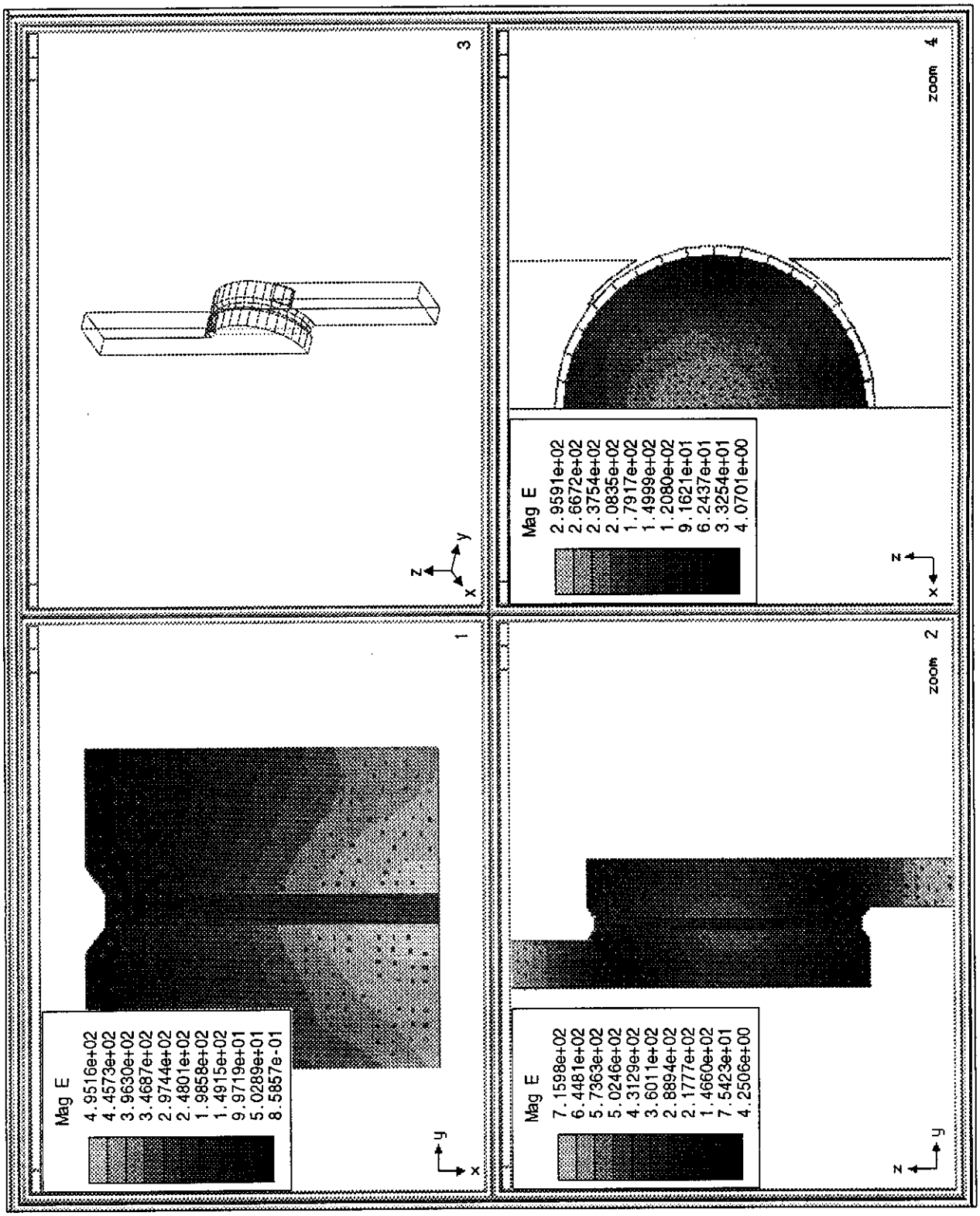

Fig.14. The field distribution in variant 1 of the window at input signal phase 0^0.

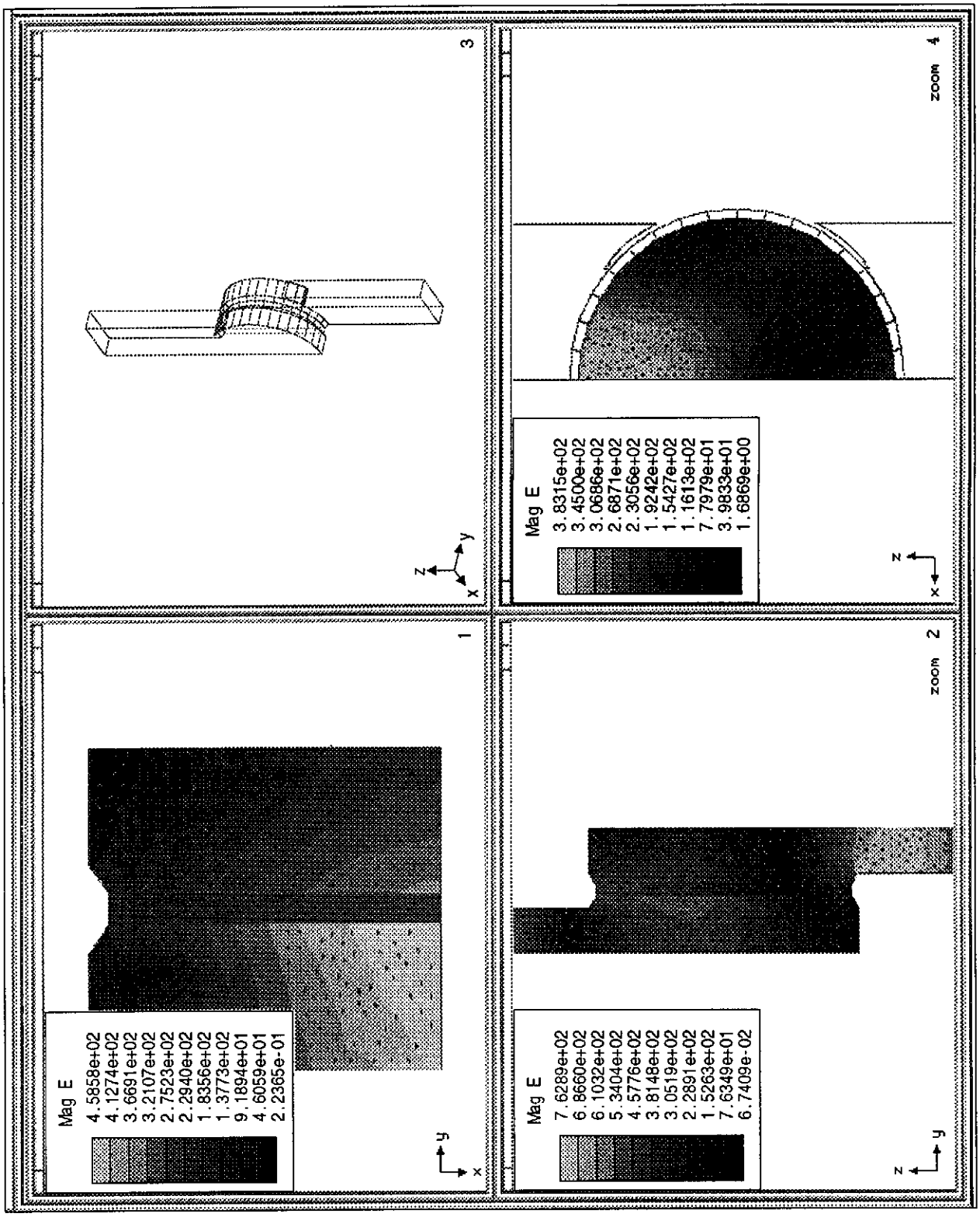

Fig.15. The field distribution in variant 1 of the window at input signal phase 30^0.

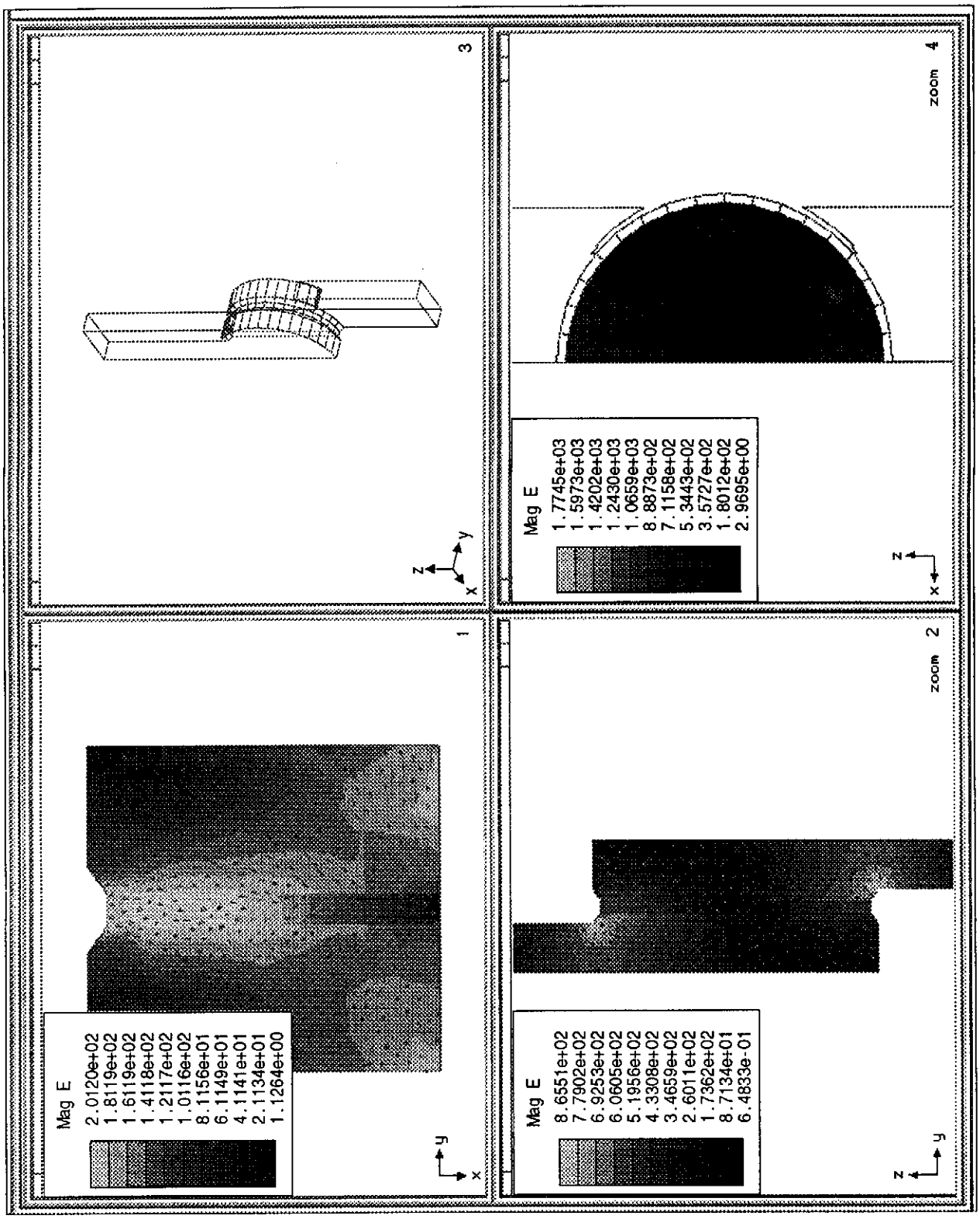

Fig.16. The field distribution in variant 1 of the window at input signal phase 90^0.

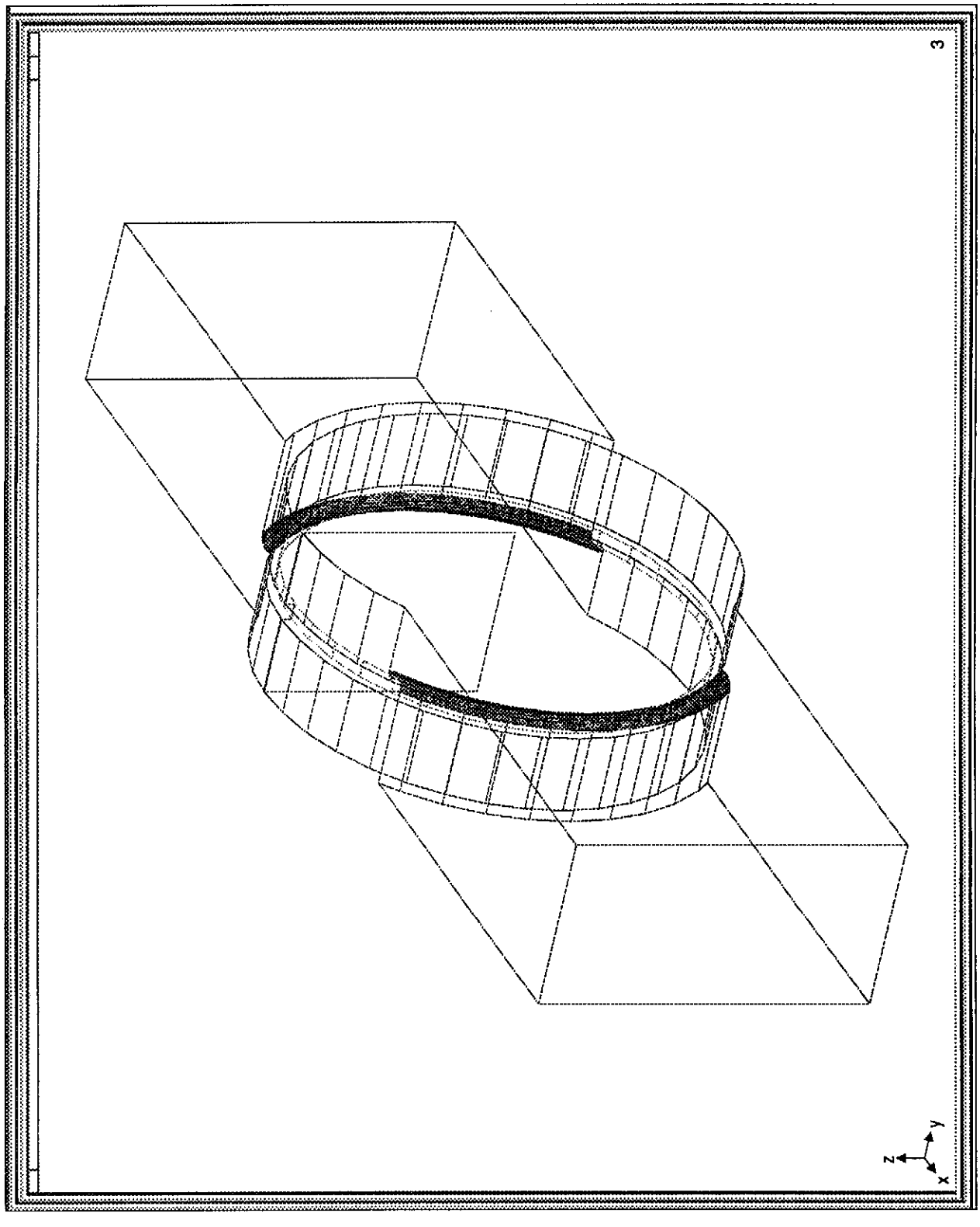

Fig.17. Variant 2 of the window.

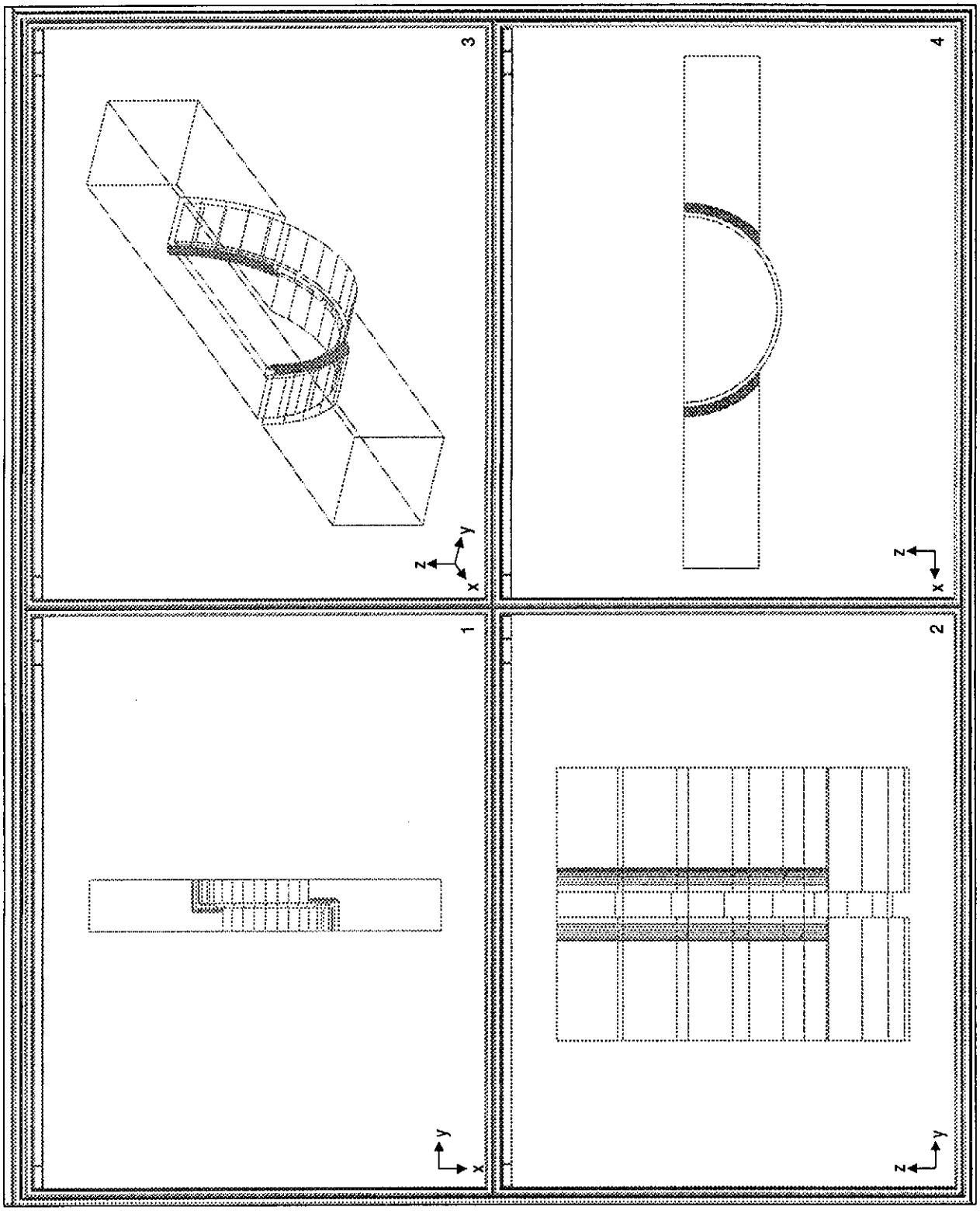

Fig.18. Variant 2 of the window.

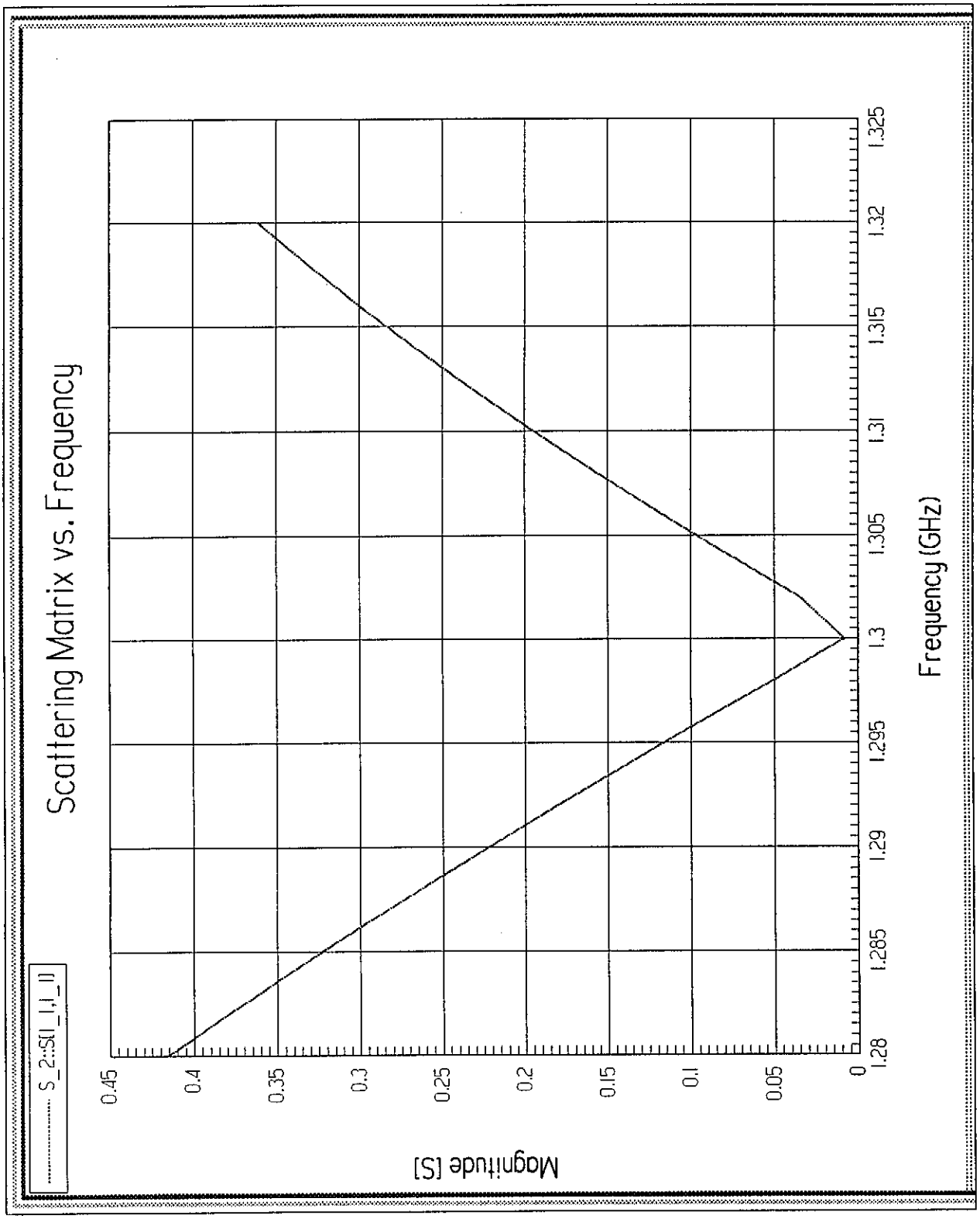

Fig.19. $S_{11}(f)$ dependence for window variant 2.

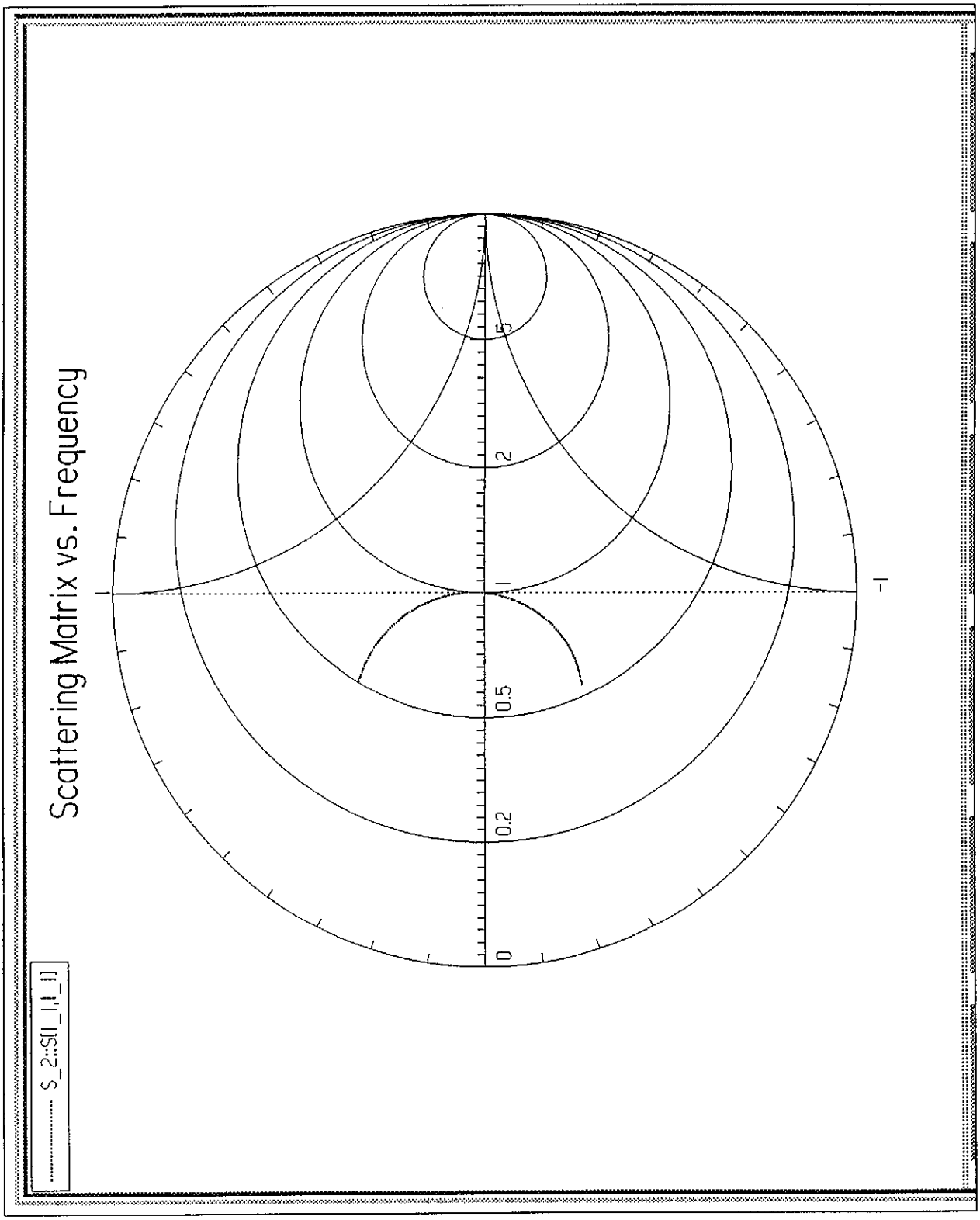

Fig.20. $S_{11}(f)$ dependence in Smith chart for window variant 2.

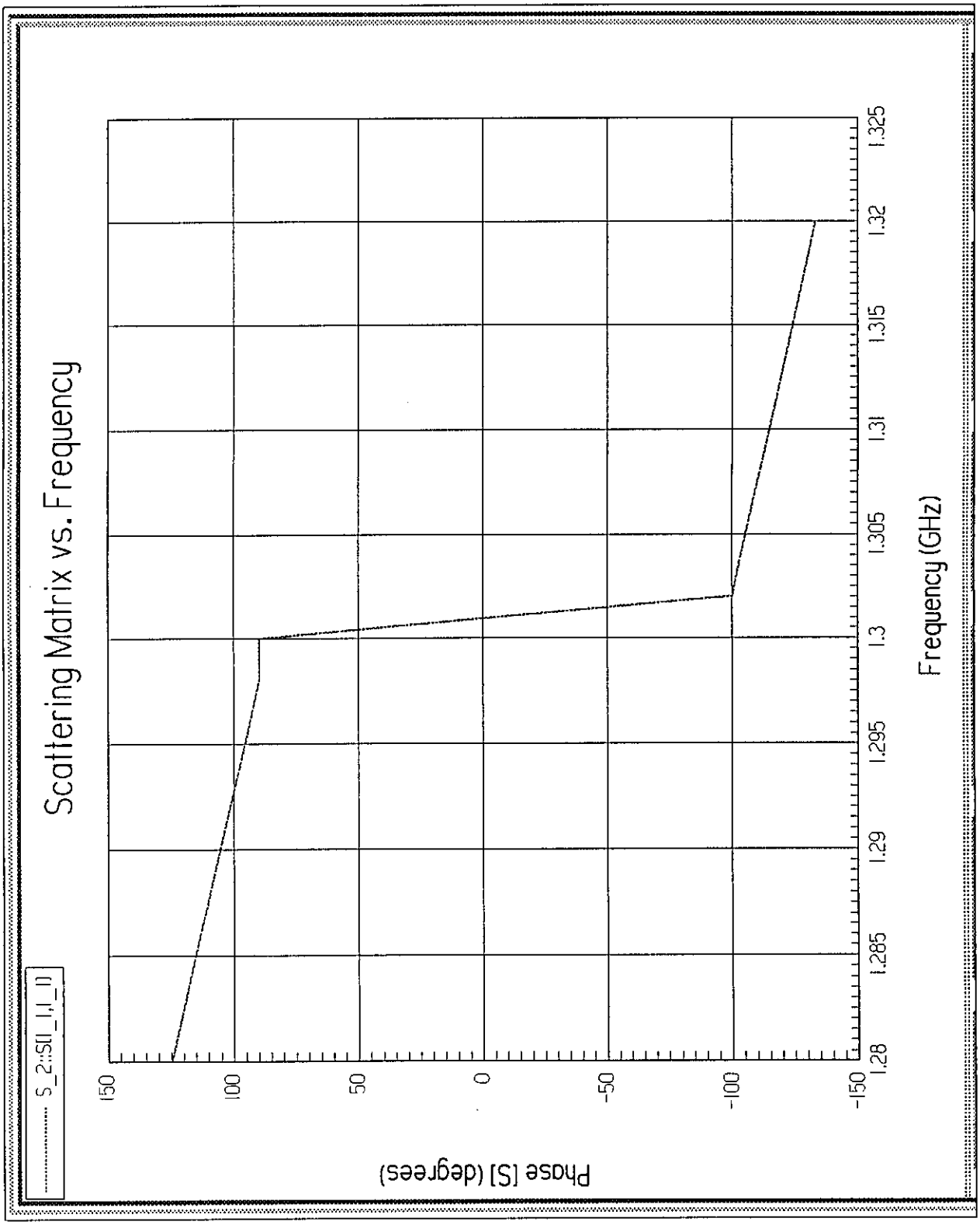

Fig.21. S_{11} phase dependence on frequency for window variant 2.

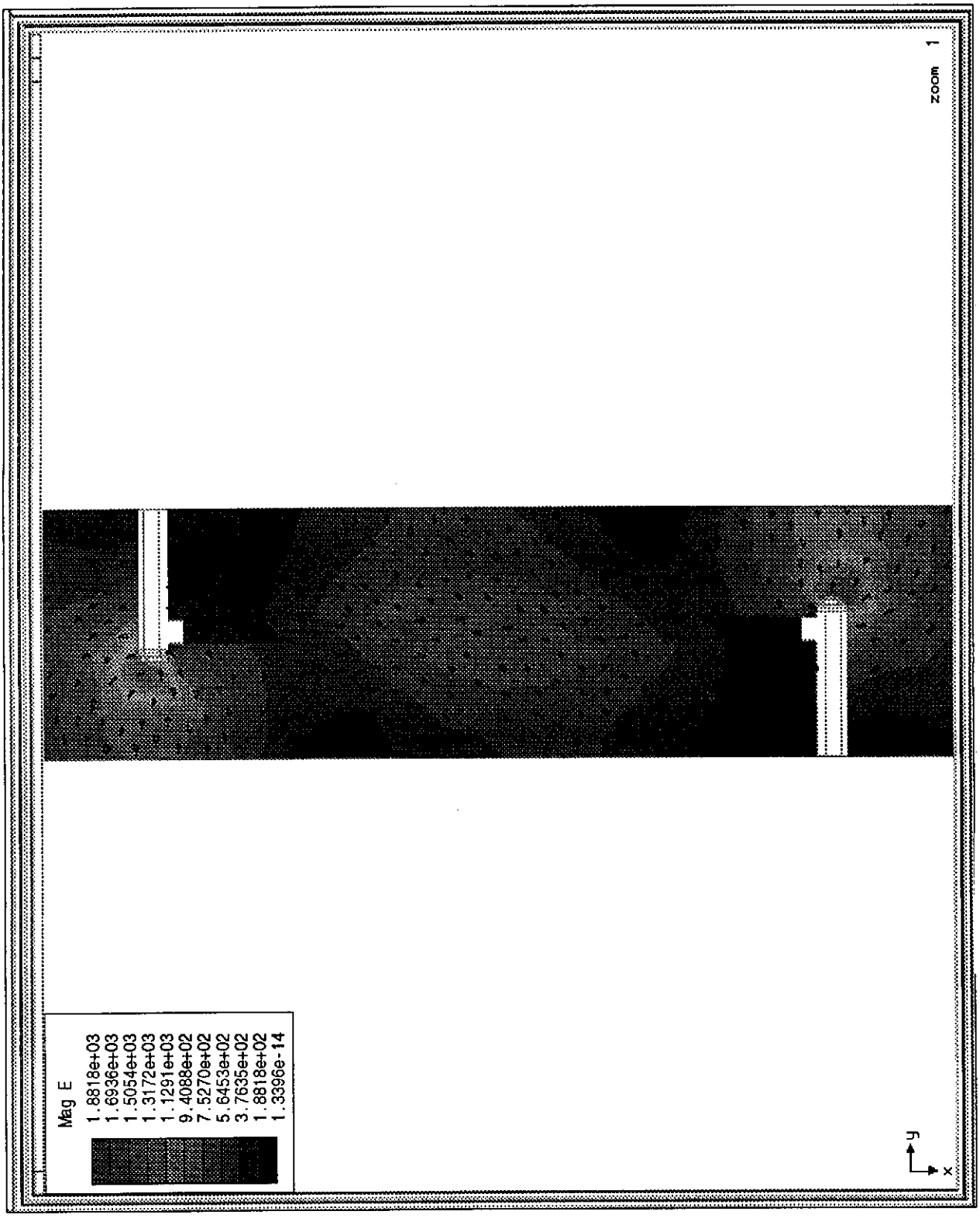

Fig.22. Electric field distribution in the window variant 2.

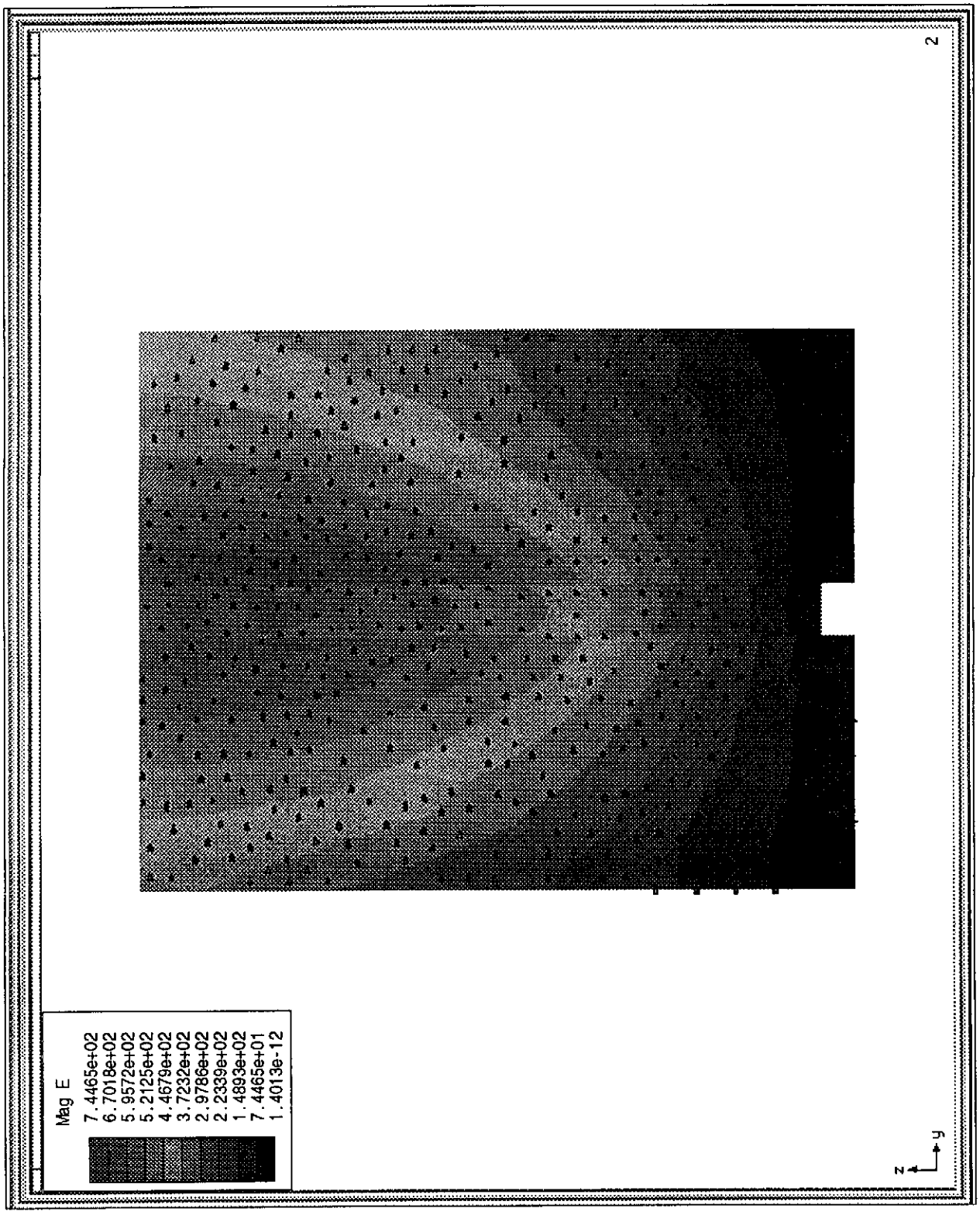

Fig.23. Electric field distribution in the window variant 2.

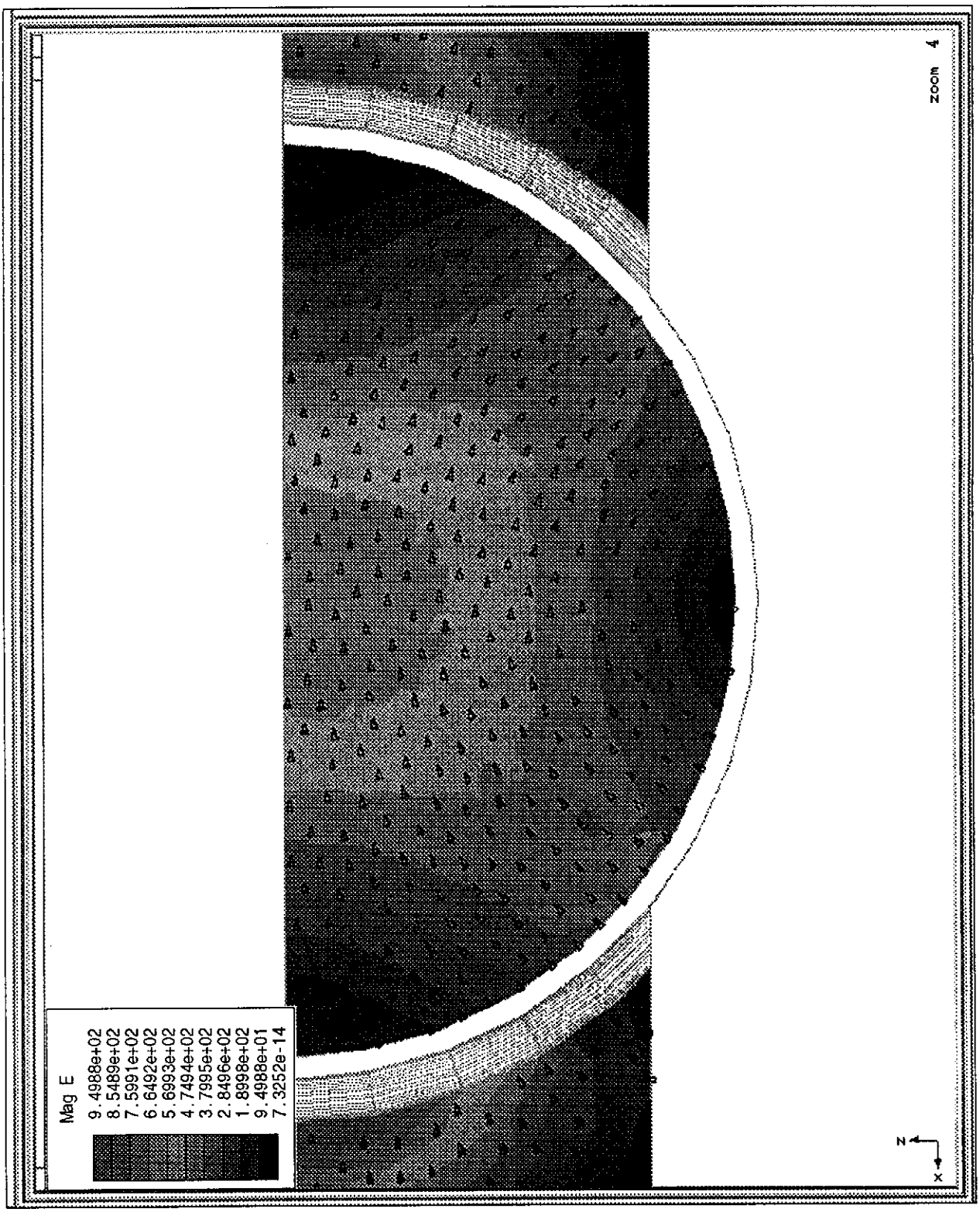

Fig.24. Electric field distribution in the window variant 2.

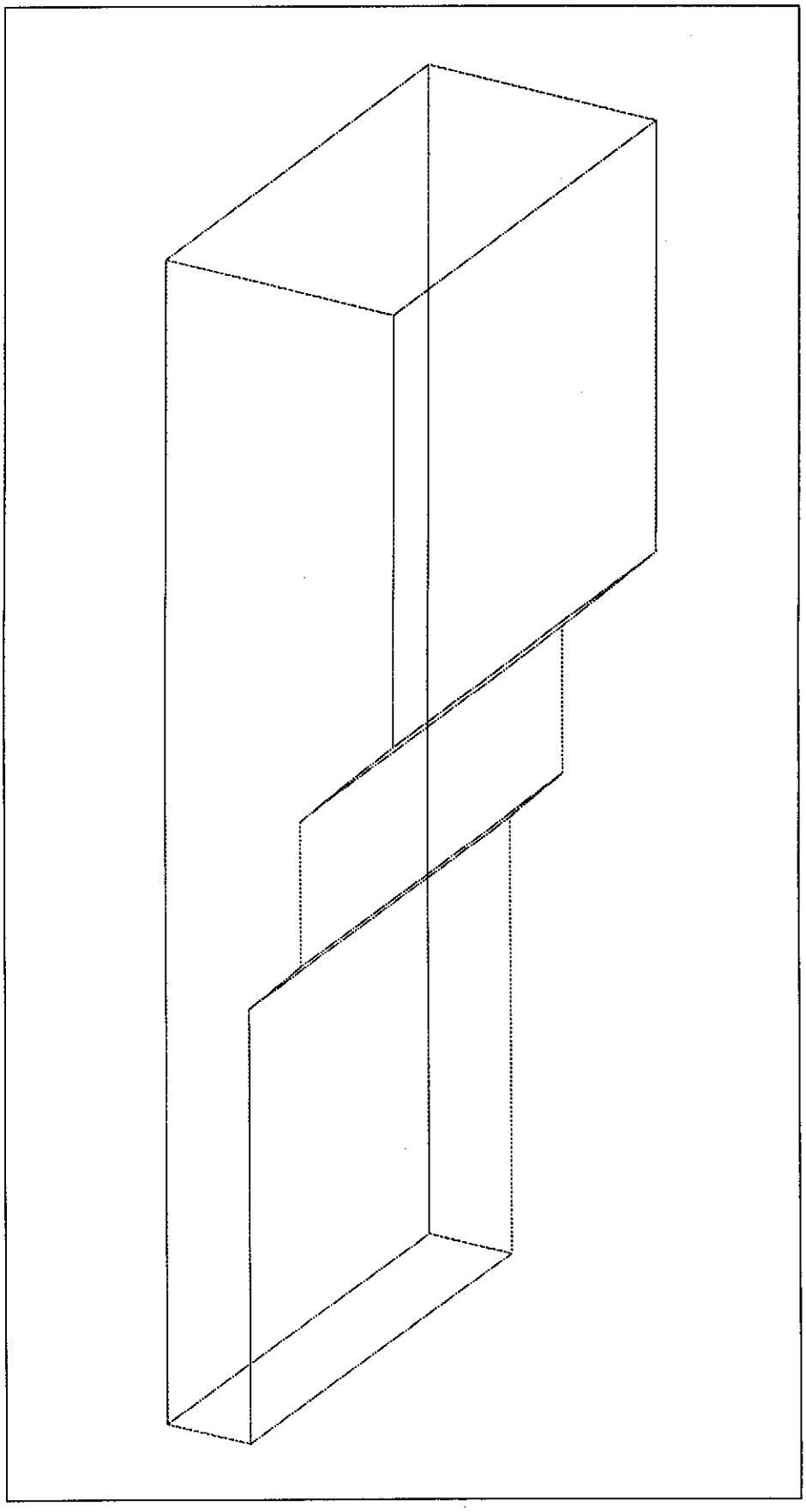

Fig.25. 82-30 mm transition.

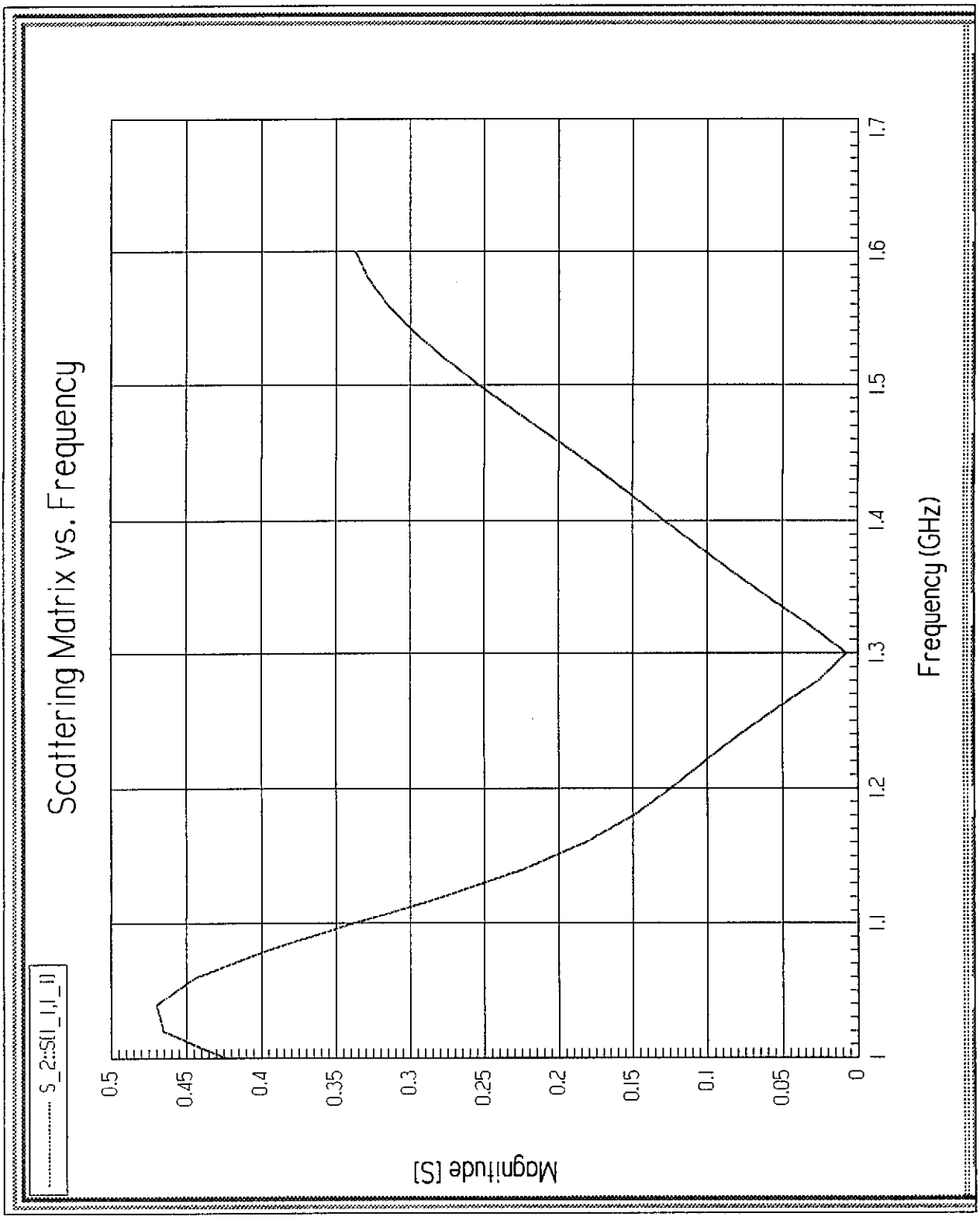

Fig.26. $S_{11}(f)$ dependence for 82x30 mm transition.

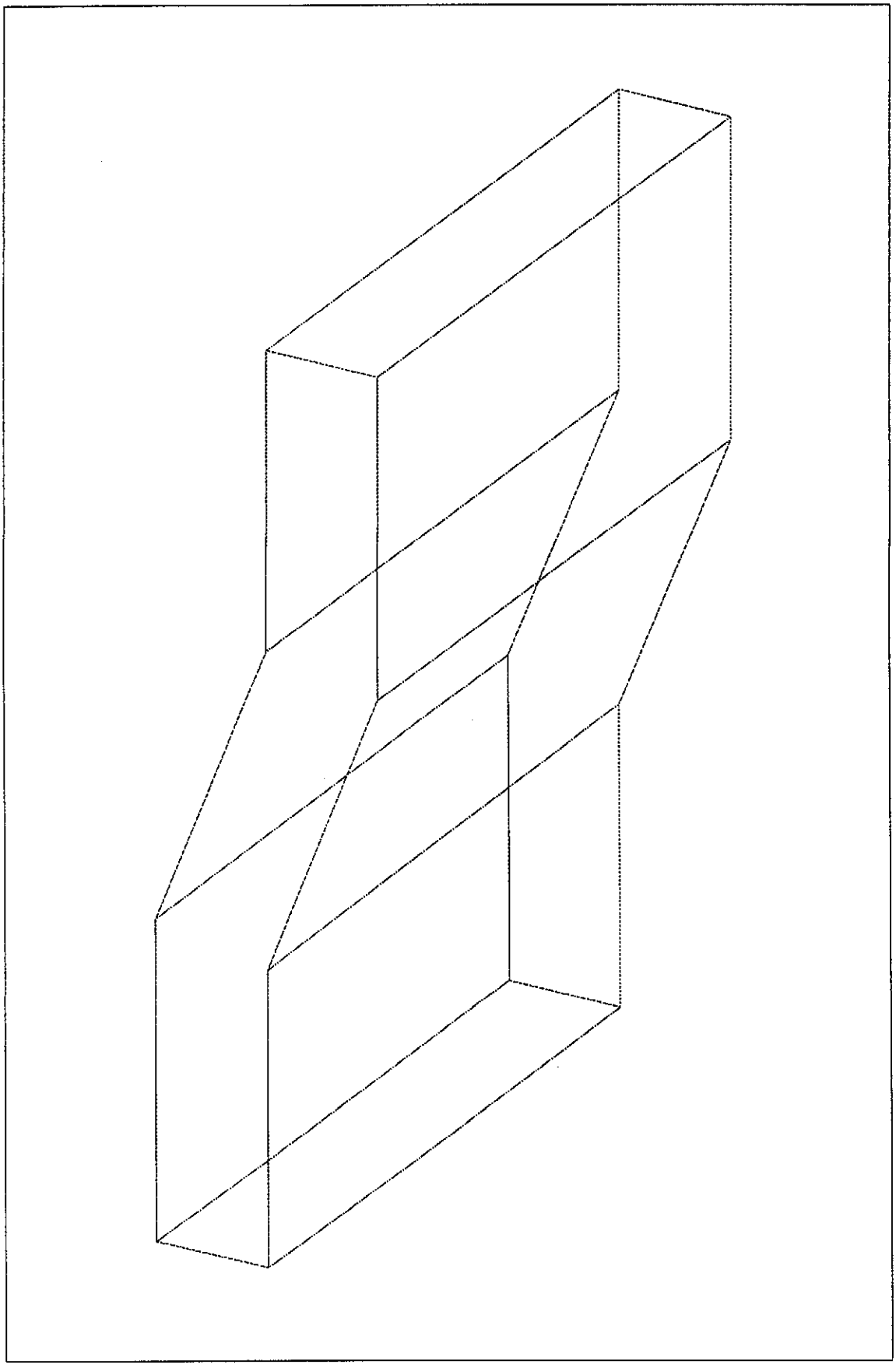

Fig.27. 30-30 mm S-bend.

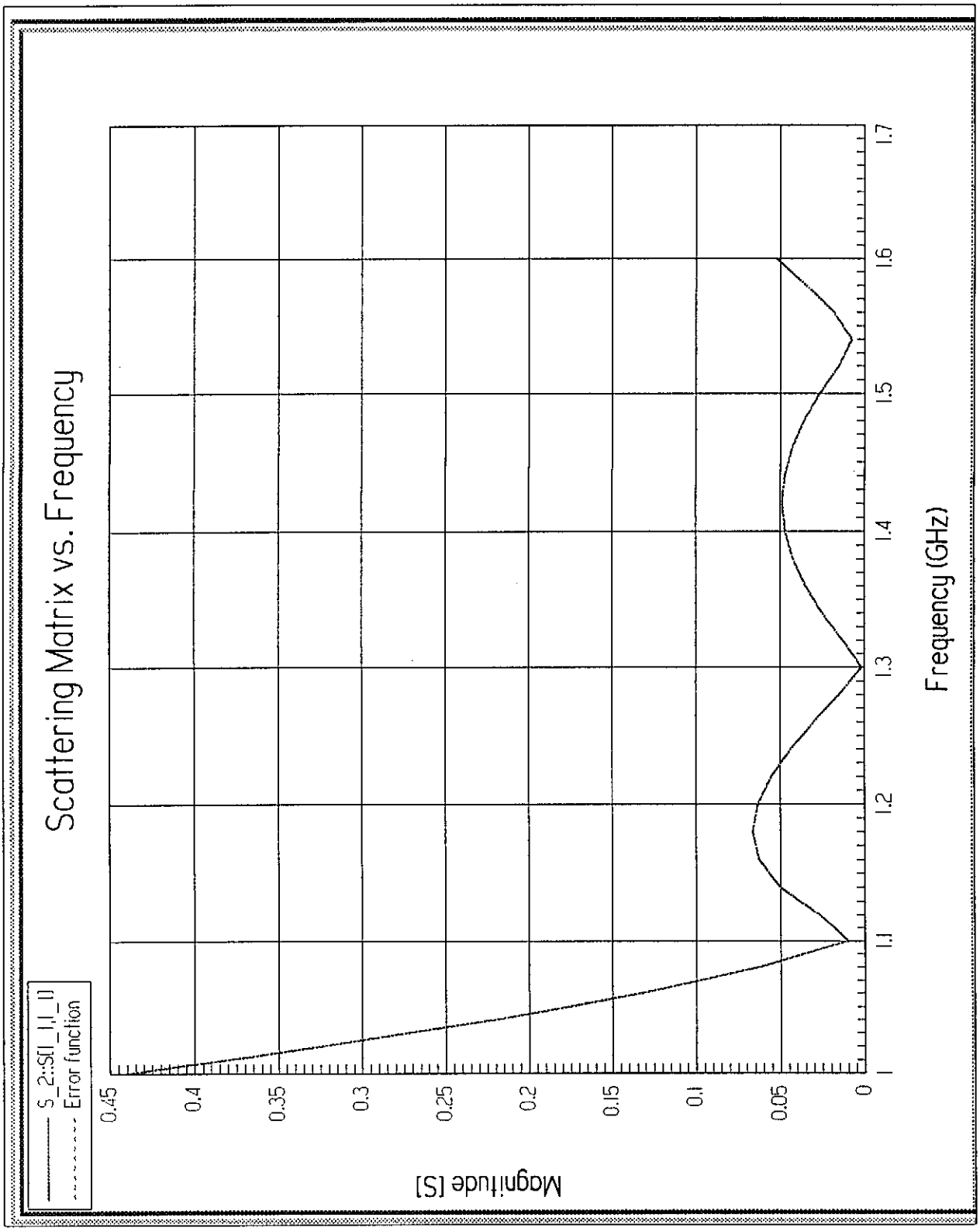

Fig.28. $S_{11}(f)$ dependence for 30-30 mm S-bend.

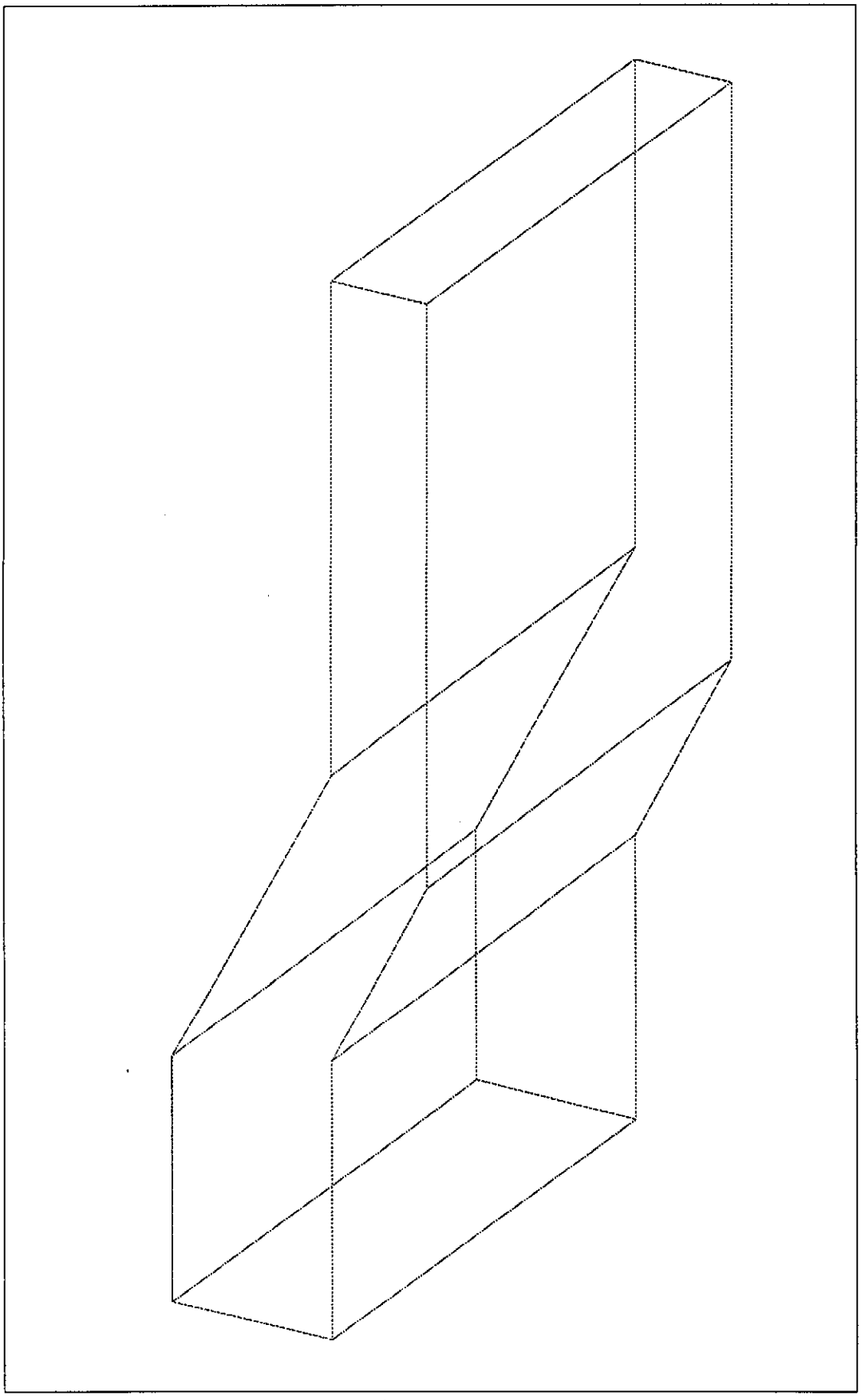

Fig.29. 30-50 mm S-bend.

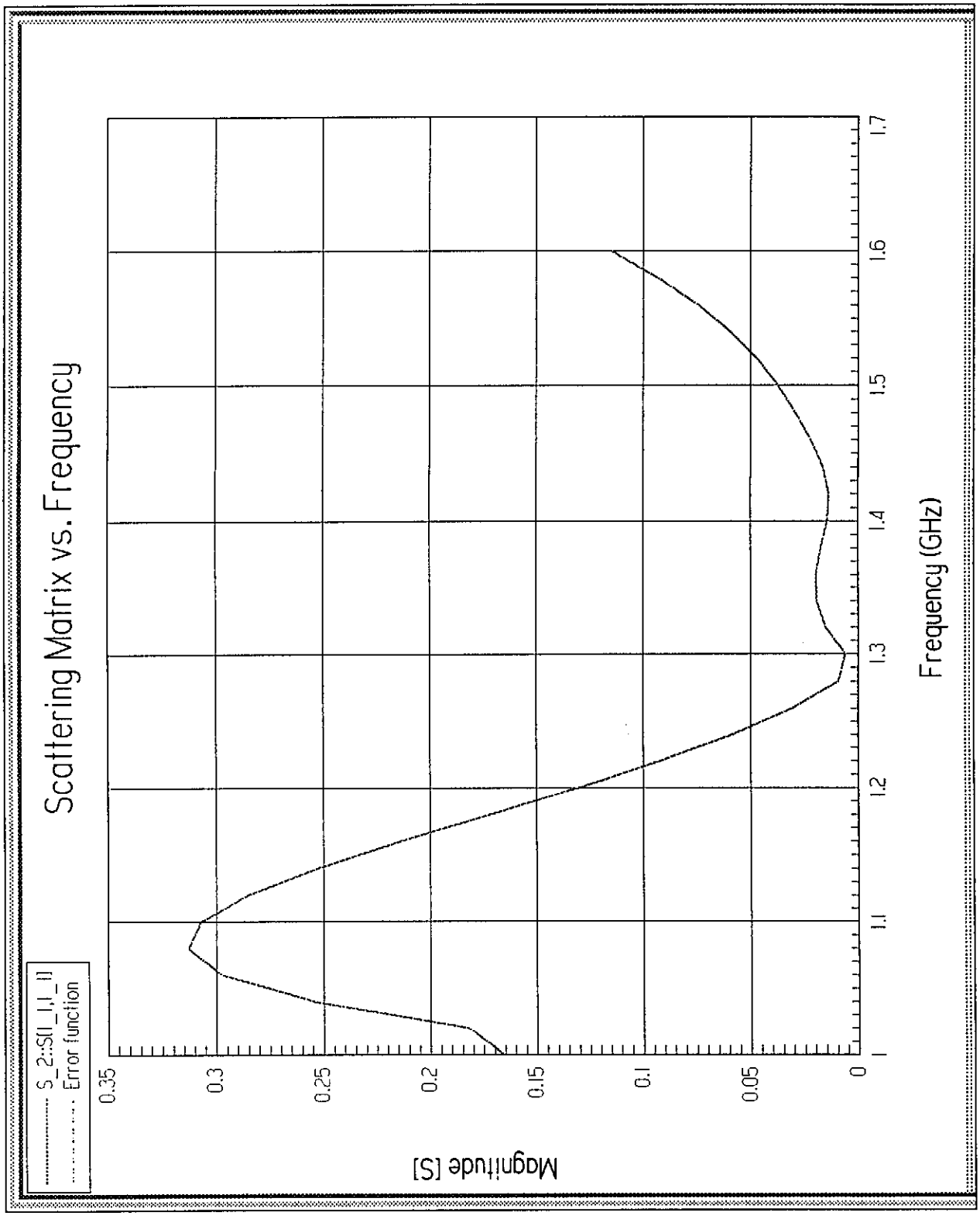

Fig.30. $S_{11}(f)$ dependence for 30-50 mm S-bend.

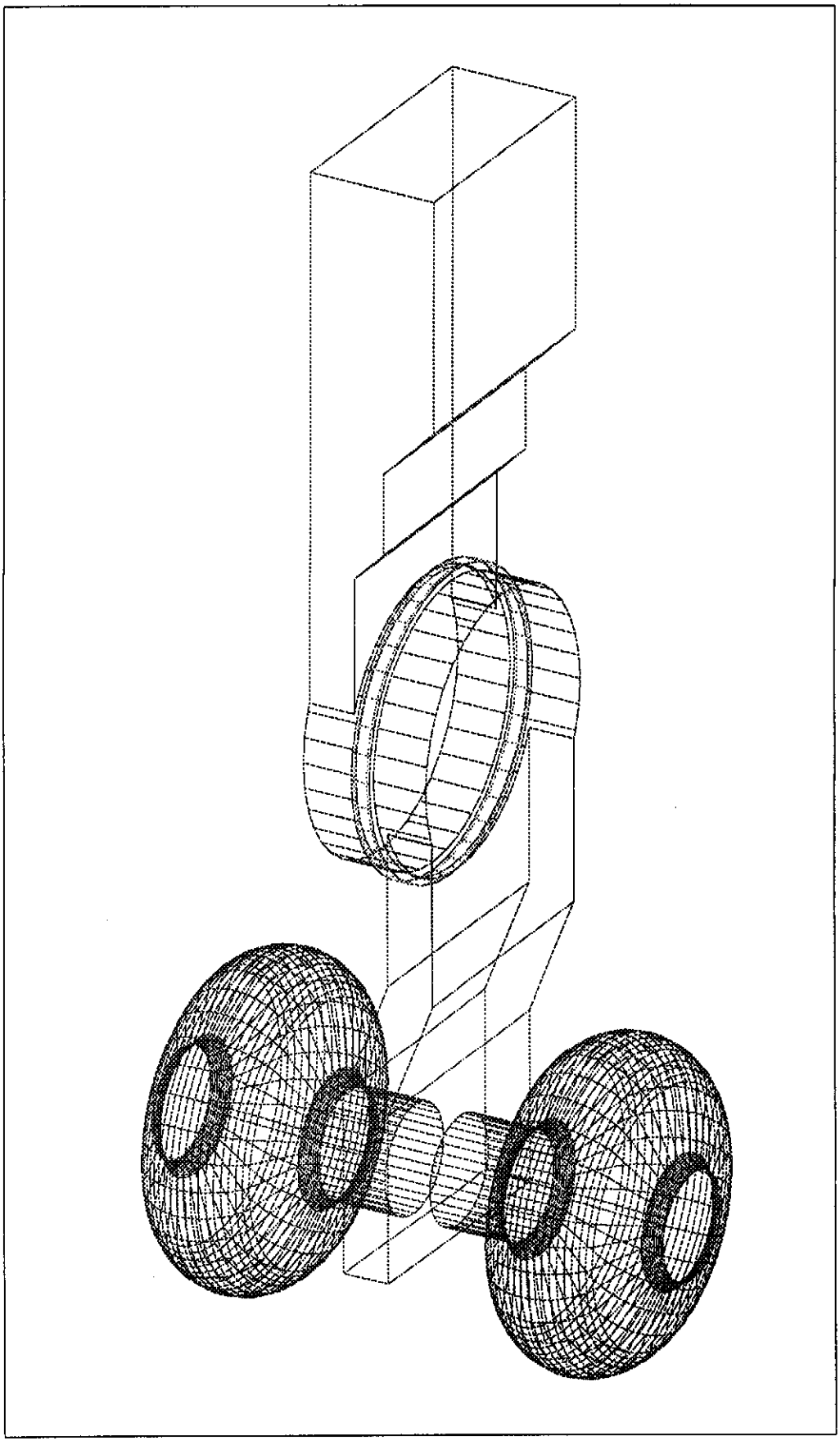

Fig.31. Common view of the coupler with the window variant 1.

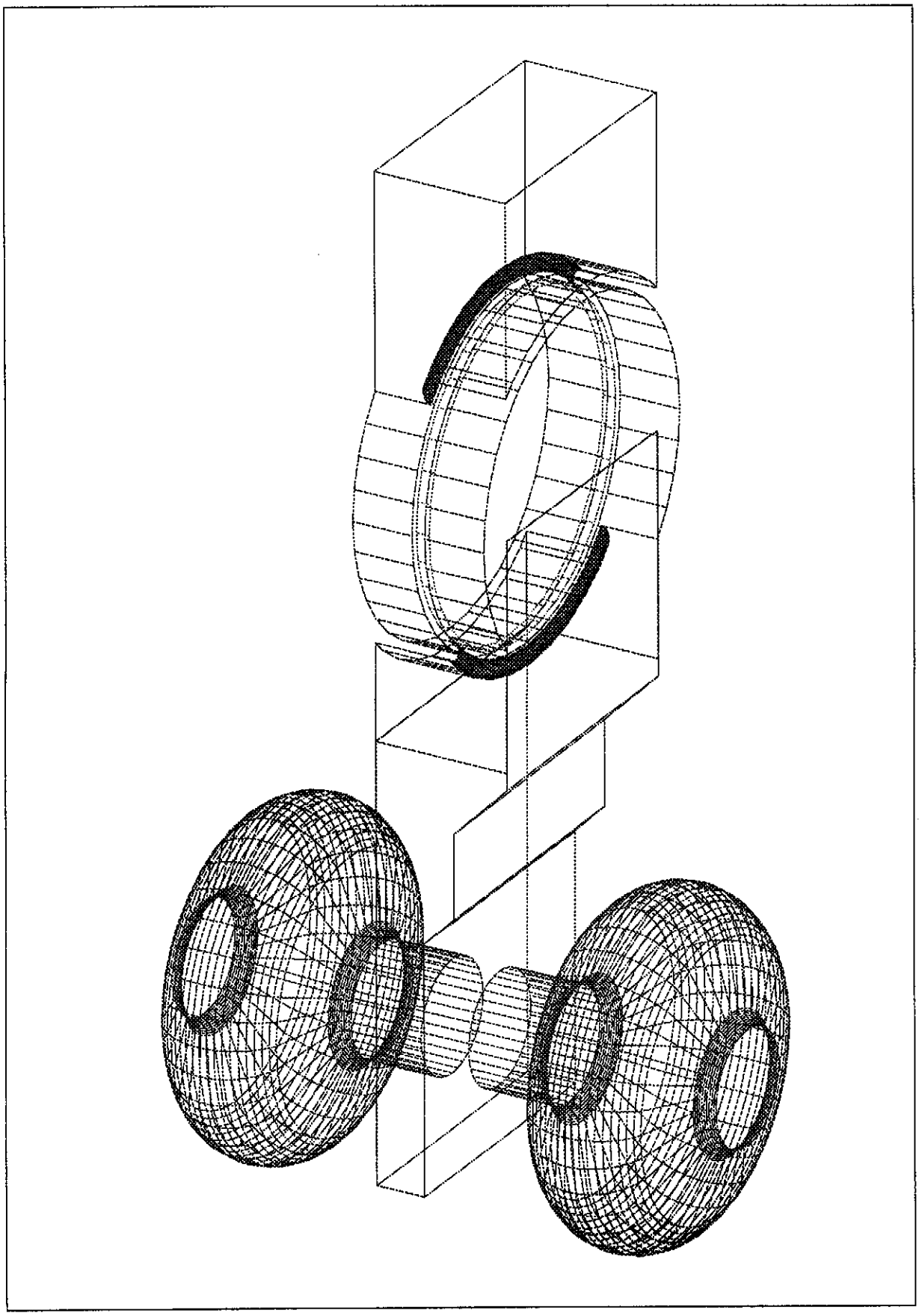

Fig.32. Common view of the coupler with the window variant 2.